

## N O T I C E

THIS DOCUMENT HAS BEEN REPRODUCED FROM  
MICROFICHE. ALTHOUGH IT IS RECOGNIZED THAT  
CERTAIN PORTIONS ARE ILLEGIBLE, IT IS BEING RELEASED  
IN THE INTEREST OF MAKING AVAILABLE AS MUCH  
INFORMATION AS POSSIBLE

Available under NASA sponsorship  
in the interest of early and wide dis-  
semination of Earth Resources Survey  
Program information and without liability  
for use or misuse thereof.

80-10232  
GR-163337

# ADVANCED SOLID STATE EARTH RESOURCES SATELLITE STUDY

## FINAL REPORT



### 30 JUNE 1980

(E80-10232) ADVANCED SOLID STATE EARTH  
RESOURCES SATELLITE STUDY Final Report  
(Eastman Kodak Co.) 70 p HC A04/MF A01

N80-29801

CSCL 22B

Unclass

G3/43

00232

1880



1980

RC-00221

*A 100-year start on tomorrow*

**ADVANCED SOLID STATE  
EARTH RESOURCES SATELLITE  
STUDY**

**FINAL REPORT  
30 JUNE 1980**

**CONTRACT NASW-3375**

Original photography may be purchased from  
EROS Data Center

Sioux Falls, SD

PREPARED BY

EASTMAN KODAK COMPANY  
RESEARCH & ENGINEERING  
ROCHESTER, NEW YORK 14650

FOR

HEADQUARTERS  
NATIONAL AERONAUTICS AND SPACE ADMINISTRATION  
WASHINGTON, DC 20546

ABSTRACT

*This report presents the findings of a sixteen week study of an advanced earth resources satellite employing linear arrays of solid state detectors. Two baseline design concepts were selected in the study: a "principal telescope" which provides optics and sensors for four visible and two short wavelength infrared bands, and a "thermal infrared telescope" which provides optics and sensors for the thermal infrared band. The telescopes are sized to cover 185 km swaths at resolutions of approximately 10 meters and 70 meters, respectively. The report presents a summary of requirements, a discussion of the selection process leading to the baseline design concepts, brief descriptions of the telescopes and their major components, and an assessment of the status of the technology needed for the satellite system and its associated ground station.*

*The study was conducted by the Government Projects group of the Kodak Apparatus Division Research and Engineering organization. George Keene was the Project Leader, assisted by James Collinge, Charles Cox, Stanley Ekiert, John Meyers, Philip Parr, Albert Rehn, and John Villa.*



## TABLE OF CONTENTS

<u>Section</u>	<u>Title</u>	<u>Page No.</u>
	<i>Title Sheet . . . . .</i>	<i>i</i>
	<i>Abstract. . . . .</i>	<i>ii</i>
	<i>Table of Contents . . . . .</i>	<i>iii</i>
	<i>List of Figures . . . . .</i>	<i>v</i>
	<i>List of Tables. . . . .</i>	<i>vi</i>
1.0	INTRODUCTION. . . . .	1
1.1	Conclusions from the Study. . . . .	3
1.2	Recommendations . . . . .	4
2.0	REQUIREMENTS, CONSTRAINTS, AND ASSUMPTIONS. . . . .	5
2.1	Operational Assumptions . . . . .	7
2.1.1	Orbital Altitude. . . . .	7
2.1.2	Pointing. . . . .	7
3.0	DATA COLLECTION AND TRADEOFF STUDIES. . . . .	10
3.1	Parametric Studies. . . . .	10
3.1.1	Parametric Relationships. . . . .	10
3.1.2	Selection of Parameters . . . . .	13
3.2	Selection of Optics . . . . .	13
3.2.1	Catadioptric Lens Configurations. . . . .	14
3.2.2	Catoptric Lens Configurations . . . . .	16
3.2.3	Thermal IR Optical Telescope. . . . .	19
3.3	Selection of Detectors. . . . .	20
3.3.1	Detector Arrays for the Visible Bands . . . . .	20
3.3.2	Detector Arrays for the Short Wavelength Infrared Bands . . . . .	21
3.3.3	Detector Arrays for the Thermal Infrared Band . . . . .	22
3.4	Configurations. . . . .	24
4.0	DESIGN APPROACH FOR THE PRINCIPAL TELESCOPE . . . . .	25
4.1	Optics. . . . .	25
4.1.1	Optical Sensitivities . . . . .	28
4.1.2	Calibration . . . . .	29
4.2	Detectors . . . . .	33
4.2.1	Introduction. . . . .	33
4.2.2	Detectors for the Visual Bands: Bands 1 - 4. . . . .	33
4.2.3	Detectors for the SWIR Bands: Bands 5 and 6. . . . .	38
4.3	Configuration . . . . .	41
4.4	Thermal Control . . . . .	43
4.5	Performance Estimates . . . . .	44
4.6	Coverage Characteristics. . . . .	46



<u>Section</u>	<u>Title</u>	<u>Page</u>
5.0	DESIGN APPROACH FOR THERMAL INFRARED TELESCOPE . . . . .	48
5.1	Optics . . . . .	48
5.2	Detectors for the TIR Band: Band 7. . . . .	49
5.2.1	Configuration. . . . .	49
5.2.2	Detector Characteristics . . . . .	50
5.3	Thermal Control. . . . .	51
5.4	Performance of the Thermal Infrared Telescope. . . . .	54
6.0	INTERFACE REQUIREMENTS . . . . .	55
6.1	Data Handling Interfaces . . . . .	56
6.2	Vehicle Interfaces . . . . .	58
7.0	PROGRAM RISK ANALYSIS. . . . .	60
7.1	Principal Telescope. . . . .	60
7.2	Thermal Infrared Telescope . . . . .	61
7.3	Ground Station . . . . .	61



## LIST OF FIGURES

<u>Figure No.</u>	<u>Title</u>	<u>Page</u>
1.0-1	Simulation of Tri-Color Resolution . . . . .	2
1.0-2	Preliminary Layout of Selected Concepts. . . . .	3
2.1.2-1	Basic Coverage Patterns. . . . .	8
2.1.2-2	Special Coverage Patterns. . . . .	8
2.1.2-3	Mirror Pointing with Two-Axis Gimbal . . . . .	9
2.1.2-4	Roll Joint Plus Single Axis Mirror Gimbal. . . . .	9
3.2.1-1	Transmitting Schmidt . . . . .	14
3.2.1-2	Maksutov . . . . .	15
3.2.1-3	Schmidt-Meniscus Cassegrain. . . . .	16
3.2.2-1	Reflecting Schmidt . . . . .	17
3.2.2-2	Reflecting Schmidt Unobstructed. . . . .	17
3.2.2-3	Walrus . . . . .	18
3.2.2-4	Inverse Schwarzschild. . . . .	18
3.2.3-1	Basic Folded "Lensless" Schmidt Concept for Thermal Telescope. . . . .	20
3.3.2-1	Percent Delta Reflectance Versus D-Star. . . . .	22
3.3.3-1	D-Star Versus Temperature TIR Detectors. . . . .	23
3.4-1	General Spacecraft Configuration Approach. . . . .	24
3.4-2	Alternate Configurations . . . . .	24
4.1-1	Principal Telescope Optics . . . . .	25
4.1.2	Inverse Schwarzschild MTF Data at 33 L/MM and 500 nm . . . . .	26
4.1-3	Schwarzschild Aspheric Tertiary Mirror . . . . .	27
4.1-4	Physical and Optical Characteristics of the Principal Telescope. . . . .	27
4.1.2-1	Calibration Device for VIS/SWIR Bands. . . . .	33
4.2.2-1	Baseline Focal Plane Array for Bands 1 - 4. . . . .	34
4.2.2-2	Relative Spectral Responsivity of Silicon CCD's for Bands 1 - 4. . . . .	35
4.2.2-3	Sensor MTF vs Spatial Frequency. . . . .	37
4.2.3-1	Baseline Focal Plane Array for Bands 5 and 6 . . . . .	38
4.2.3-2	HgCdTe Spectral Responsivity . . . . .	39
4.2.3-3	SWIR Sensor MTF. . . . .	40
4.3-1	Principal Telescope. . . . .	41
4.3-2	Roll Joint Design Concept. . . . .	42
4.4-1	Principal Telescope Thermal Control. . . . .	43
4.5-1	Performance for VIS Telescope. . . . .	45
4.5-2	Performance for SWIR Telescope . . . . .	45
4.6-1	Typical Coverage Patterns. . . . .	47
5.0-1	TIR Telescope. . . . .	48
5.1-1	Diffraction Image Size at Wavelength 11.5 $\mu$ . . . . .	49
5.2.1-1	TIR Detectors. . . . .	50
5.2.2-1	Normalized Spectral Responsivity . . . . .	51
5.2.2-2	TIR Detector MTF . . . . .	51
5.3-1	TIR Thermal Control. . . . .	52
5.3-2	Thermal Control for TIR Detectors. . . . .	53



<u>Figure No.</u>	<u>Title</u>	<u>Page</u>
5.4-1	Performance for TIR Telescope . . . . .	54
6.0-1	Operational Interfaces . . . . .	55
6.1-1	Typical Data Flow (Each Visible Channel) . . . . .	56
6.1-2	On-Board Data Flow . . . . .	57
6.1-3	On-Ground Data Flow. . . . .	58
6.2-1	Vehicle Interfaces . . . . .	59
6.2-2	Shuttle Mounting Plan. . . . .	59



**LIST OF TABLES**

<u>Table No.</u>	<u>Title</u>	<u>Page</u>
2.0-1	Derived Parameters . . . . .	6
3.1.1-1	Irradiance at the Satellite. . . . .	12
4.1.1-1	Principal Optical Telescope Sensitivities. . . . .	28
4.2.2-1	Silicon CCD Detector Characteristics . . . . .	36
4.2.3-1	PV, HgCdTe Detector Characteristics. . . . .	39
4.3-1	Principal Telescope Components . . . . .	43
5.2.2-1	TIR PV, HgCdTe Detector Characteristics. . . . .	51



## 1.0 INTRODUCTION

This report presents the findings of a 16-week study of advanced earth resources sensing systems, conducted by the Apparatus Division of Eastman Kodak Company for NASA Headquarters under Contract NASW-3375. A design concept was selected during the study for a multispectral imaging system which is based on the use of linear arrays of solid-state photo detectors that sample an image of the earth as it passes below the spacecraft. No moving parts are required during imaging, but roll and stereo pointing capabilities are included to provide flexibility in coverage programming. The advanced system should provide an eight-fold resolution improvement over Landsat A, as shown in Figure 1.0-1.

The study was based in part on a prior Kodak study, conducted in 1971 for the NASA Goddard Space Flight Center\*. The current study extended and updated the survey of linear detector arrays conducted in the GSFC study, and included investigation of optics and sensors for the 1.5- to 2.4-micrometer and 10.5- to 12.5-micrometer infrared spectral regions, as well as the visible bands.

Two telescope design concepts were selected: a "principal telescope", which provides optics and sensors for the visible and short wavelength infrared bands, and a "thermal infrared telescope", which provides optics and sensors for the longer wavelength infrared band. A preliminary layout of the selected concepts is shown in Figure 1.0-2.

This report presents a summary of the requirements given or assumed for the study, a discussion of the selection process by which the principal and TIR telescopes baselines were chosen, descriptions of the selected telescope design concepts, and a brief assessment of the status of the technology needed for the satellite system and its associated ground station.

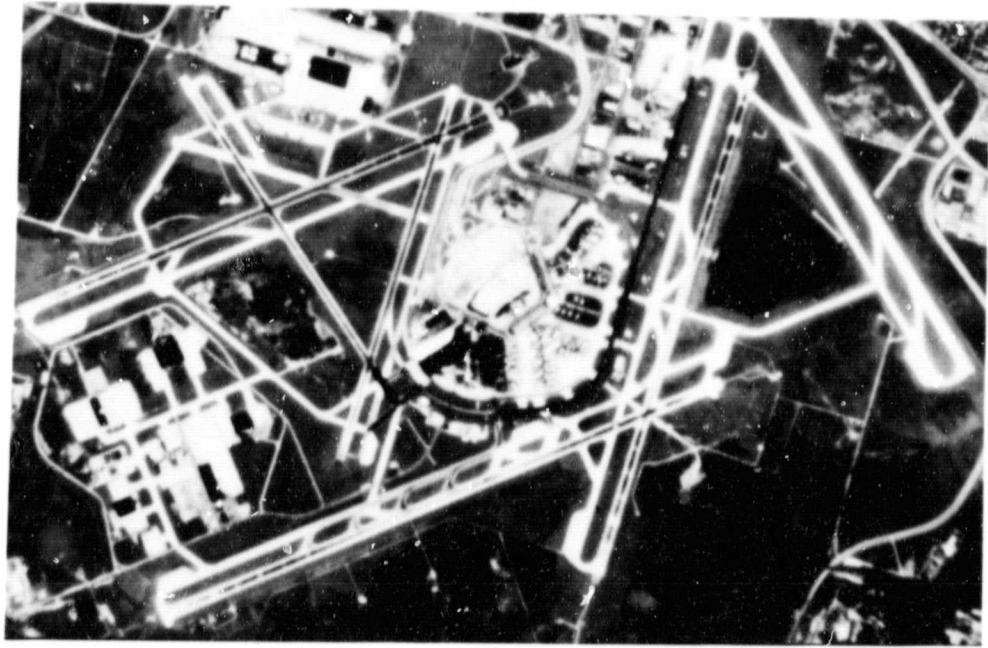
---

\*NAS5-21595, "Multispectral Imaging System Study", September 1971.



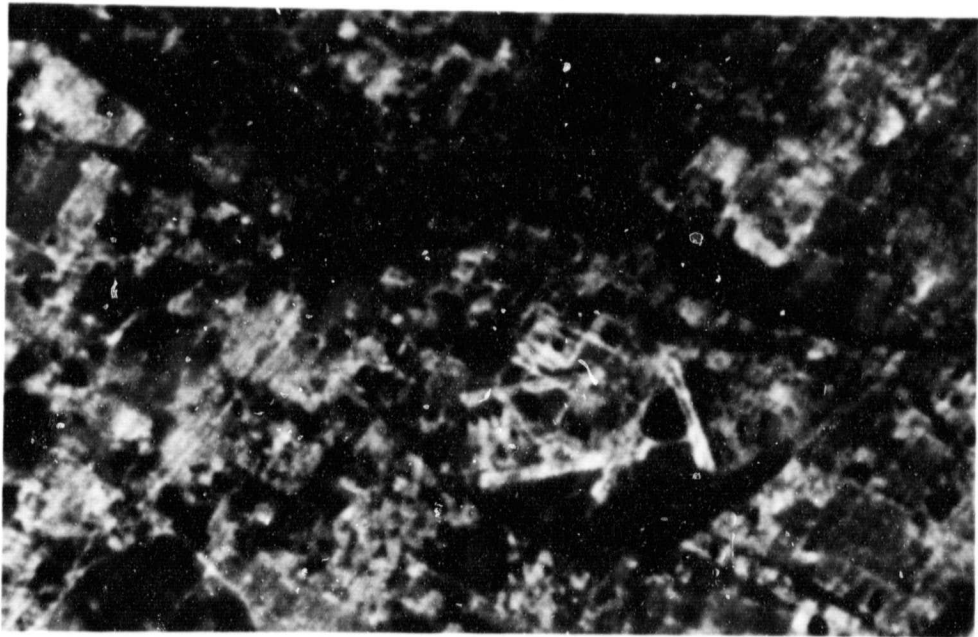
**SIMULATION OF**  
**TRI-COLOR RESOLUTION**

*Figure 1.0-1*

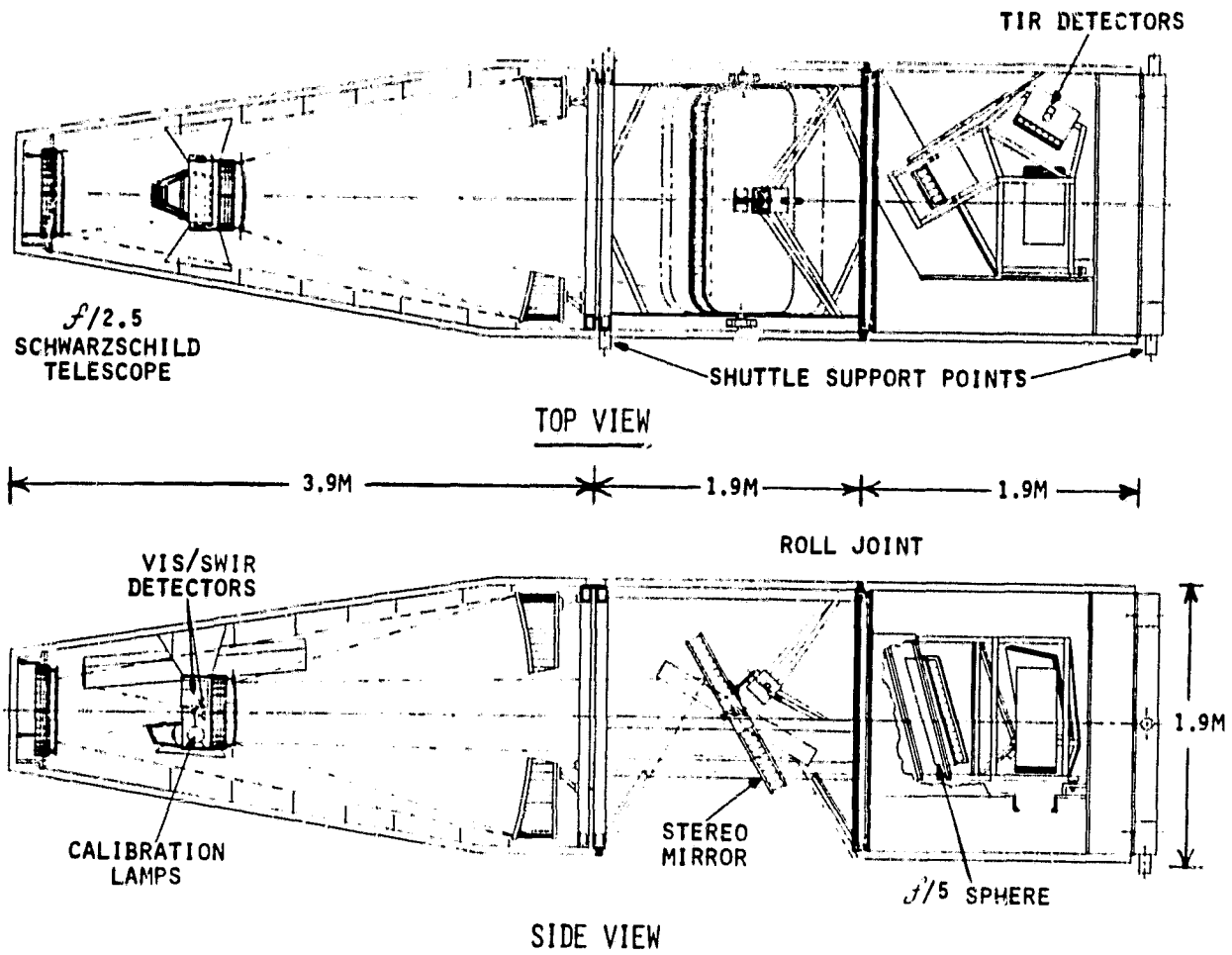


ADVANCED  
SYSTEM

ORIGINAL PAGE IS  
OF POOR QUALITY



LANDSAT A



PRELIMINARY LAYOUT OF SELECTED CONCEPTS

Figure 1.0-2

1.1 CONCLUSIONS FROM THE STUDY

A. A linear array imaging system has been defined that offers the following:

- Seven spectral bands from 0.35 to 12.5 microns
- Improved resolution (10-meter IFOV, visual)
- Intrinsic pixel registration



- Stereo and roll pointing
  - Extended life--up to five years
- B. The concept is inherently reliable and is manufacturable with existing facilities.
- No moving parts during imaging
  - No critical tolerances or environments
  - Proven optical and near-term sensor technology
  - Reasonable performance margins in each spectral band
  - Nominal spacecraft support requirements

## 1.2 RECOMMENDATIONS

The study has established baseline design concepts for the imaging components of an advanced earth resources satellite. It has not established their development cost and schedule, nor has it established the equipment requirements, and cost and schedule for the associated ground data processing and recording equipment. It is recommended, therefore, that the study be extended to include the following efforts:

- A. Establish a set of performance requirements for the overall system (satellite sensing system and ground reconstruction system).
- B. Establish a design baseline for the satellite sensing system, and develop cost and schedule estimates (ROM) for its development.
- C. Establish a design baseline for the ground reconstruction equipment (hardware and software), and develop cost and schedule estimates (ROM) for development.



## 2.0 REQUIREMENTS, CONSTRAINTS, AND ASSUMPTIONS

The initial requirements for the study as given by NASA were:

<u>SPECTRAL BAND (MICROMETERS)</u>	<u>IFOV (METERS)</u>	<u>SENSITIVITY*</u>
.35 - .50	10	0.8% NE $\Delta$ R
.50 - .62	10	0.5% NE $\Delta$ R
.62 - .70	10	0.5% NE $\Delta$ R
.74 - 1.0	10	0.5% NE $\Delta$ R
1.55 - 1.75	20	1.0% NE $\Delta$ R
2.10 - 2.40	20	2.4% NE $\Delta$ R
10.5 - 12.5	TBD	0.5 <sup>0</sup> K NE $\Delta$ T
GROUND SWATH	185 KM	
STEREO COVERAGE	$\pm 15^0$	
MAXIMUM ROLL	$\pm 3$ SWATHS	

Two orbits were to be considered, both of which provide sun synchronism. From these given requirements and orbital constraints, a set of system parameters can be derived. Table 2.0-1 lists derived system parameters for these orbits.

The following constraints were imposed on the system design:

- a. Size and Weight - Compatible with Shuttle launch into polar orbit and with the MMS (goal).
- b. Data Bandwidth - 300 megabits/second maximum.
- c. Lifetime - Two years (required), five years (goal).

In addition to the above requirements and constraints provided by NASA, Kodak established the following design objectives for the study:

- a. Stabilized spacecraft for simple interfaces
  - No vehicle pointing
  - Mechanically and thermally isolated payload

---

*\*From Thematic Mapper specification, NE $\Delta$ R is noise equivalent reflectance difference and NE $\Delta$ T is a noise equivalent temperature difference.*



Table 2.0-1  
DERIVED PARAMETERS

ORBIT	ALTITUDE INCLINATION PERIOD GROUND VELOCITY	705 KM 98.2° 98.6 MIN 6.74 KM/SEC	920 KM 98.2° 101.1 MIN 6.47 KM/SEC
OPTICS	FIELD COVERAGE (FULL) ROLL ANGLES 1 SWATH OFFSET 2 SWATHS OFFSET 3 SWATHS OFFSET FOCAL LENGTH	14.96°  14.7° 27.7° 38.2° 1058 MM*	11.48°  11.4° 21.9° 31.0° 1380 MM*
DETECTORS VISIBLE	SIZE # PER CHANNEL INTEGRATION TIME SAMPLING RATE/ BAND LENGTH NYQUIST FREQUENCY	15x15 MICROMETERS 18,500 1.48 MS  12.5x10 <sup>6</sup> /SEC .277 METER 33.3 CPMM	15x15 MICROMETERS 18,500 1.55 MS  11.93x10 <sup>6</sup> /SEC .277 METER 33.3 CPMM
SHORT WAVELENGTH INFRARED	SIZE # PER BAND LENGTH INTEGRATION TIME SAMPLING RATE/ BAND NYQUIST FREQUENCY	25x30 MICROMETERS <sup>†</sup> 9,250 .277 METER 2.47 MS  3.74x10 <sup>6</sup> /SEC 16.7 CPMM	25x30 MICROMETERS <sup>†</sup> 9,250 .277 METER 2.58 MS  3.58x10 <sup>6</sup> /SEC 16.7 CPMM
THERMAL INFRARED	SIZE # PER BAND LENGTH INTEGRATION TIME SAMPLING RATE/ BAND NYQUIST FREQUENCY	100x105 MICROMETERS <sup>‡</sup> 2,664 277.5 MM 9.87 MS  270x10 <sup>3</sup> /SEC 5 CPMM	100x105 MICROMETERS <sup>‡</sup> 2,664 277.5 MM 10.33 MS  258x10 <sup>3</sup> /SEC 5 CPMM
<p>*Selected for 10-meter IFOV with 15 micrometer detector.  <sup>†</sup>Includes 5 micrometer spacing between detectors.  <sup>‡</sup>From TIRA specification; includes 5 micrometers spacing between detectors.</p>			



- b. Intrinsic Reliability
  - Passive cooling
  - Minimum moving parts (no moving parts during imaging)
- c. Intrinsic Registration
  - Pushbroom array, close spacing of spectral bands
- d. Minimum Development Risk
  - Available optical, detector, and thermal control technologies
  - Minimum control tolerances
  - Conventional factory testing
  - Straightforward operational calibration
  - Modular thermal IR package

## 2.1 OPERATIONAL ASSUMPTIONS

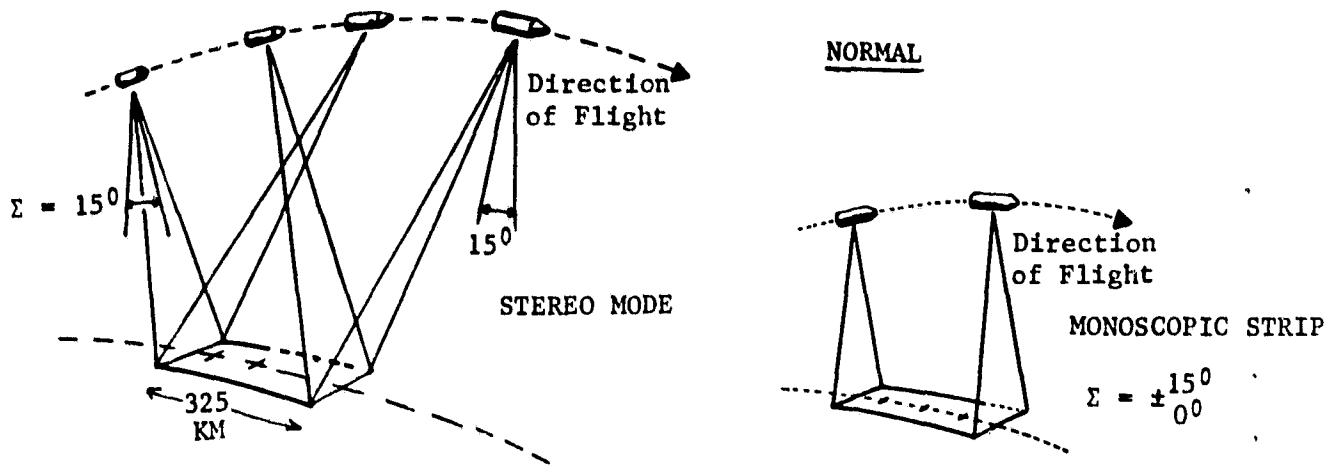
### 2.1.1 Orbital Altitude

The lower of the two candidate operational orbits was selected as the baseline for the purpose of this study. This choice was made arbitrarily and should be reviewed as part of a more detailed system design study. Rationale for the lower orbit includes lower propellant requirements for orbit injection and return to the shuttle orbit for retrieval, and reduced optical size for the required resolution. Rationale for the higher orbit includes more frequent access to ground areas and a smaller angular optical field for the required swath coverage. The analyses of this study are based on parameters associated with the lower orbit.

### 2.1.2 Pointing

An important new feature of the advanced system is the capability for both in-track and cross-track pointing. The former permits stereo coverage of selected areas, while the latter provides the capability for more frequent coverage of high priority areas. This stereo capability is illustrated in Figure 2.1.2-1.

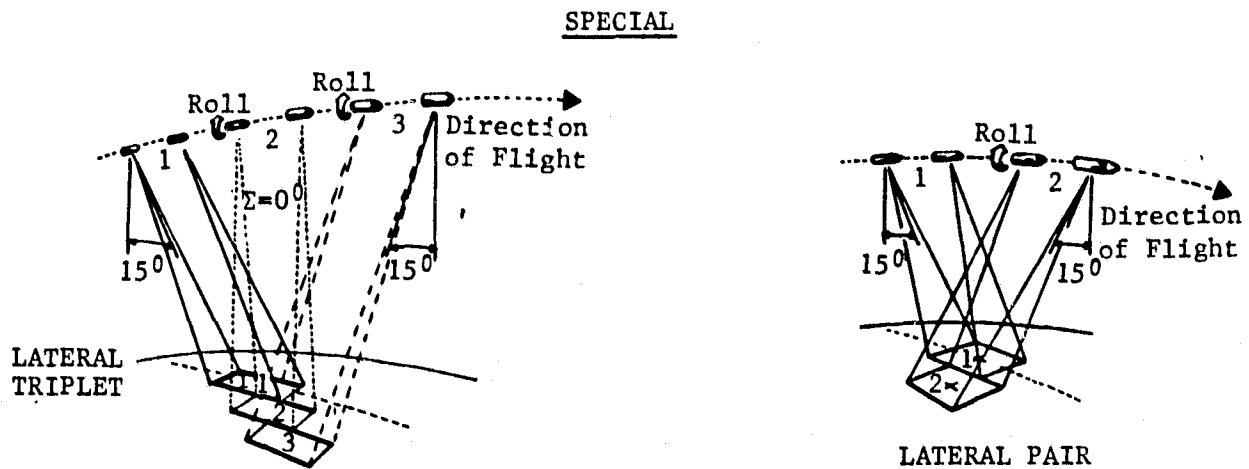




BASIC COVERAGE PATTERNS

Figure 2.1.2-1

In combination, the in-track and cross-track pointing capability can also be used to provide "lateral pair" and "lateral triplet" coverage of selected areas, as shown in Figure 2.1.2-2.

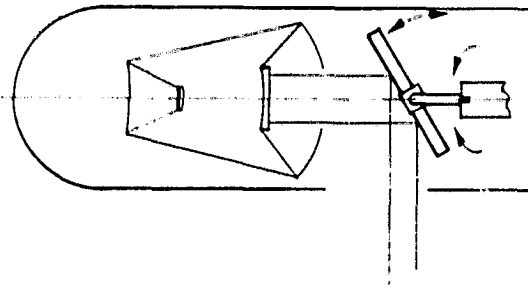


SPECIAL COVERAGE PATTERNS

Figure 2.1.2-2



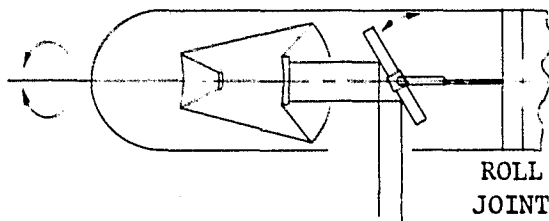
Two pointing approaches were considered, both compatible with the objective of minimum perturbation of the spacecraft. Figure 2.1.2-3 shows an approach which uses a two-axis, gimballed pointing mirror. One drawback of this approach is that the focal plane must also be rotated to keep the image velocity vector normal to the line of detectors. The viewport opening in the spacecraft must be very large to accommodate the full range of pointing on both axes, complicating thermal control of the optics.



MIRROR POINTING WITH  
TWO-AXIS GIMBAL

Figure 2.1.2-3

A second approach, which avoids rotation of the focal plane and minimizes the viewport size, is shown in Figure 2.1.2-4. For cross-track pointing, in this approach, the whole optical sensing system is rotated by means of a "roll joint" which is internally compensated to minimize disturbance to the spacecraft. This method has only one serious drawback--the sensing system does not maintain a constant orientation with respect to cold space; therefore, use of a space radiator is compromised. This consideration, as well as other problems associated with maintaining a thermal infrared sensor in the same environment with the visible and short wavelength infrared sensors, led to a decision early in the study to include only the latter two sensors in the pointable telescope and to provide a separate fixed telescope for the thermal infrared sensor (see Section 3.2.3).



ROLL JOINT PLUS SINGLE  
AXIS MIRROR GIMBAL

Figure 2.1.2-4

### 3.0 DATA COLLECTION AND TRADEOFF STUDIES

One of the principal objectives of this study was to select design approaches and design parameters compatible with the near-term state-of-the-art in each design area. To aid in making state-of-the-art assessments, a brief parametric study was conducted to establish approximate design values. A survey of available literature and vendors was then conducted to identify candidate materials, components, and design approaches. These efforts are described in the following paragraphs.

#### 3.1 PARAMETRIC STUDIES

##### 3.1.1 Parametric Relationships

The basic system performance equations for each spectral region are:

##### 1. Visible Bands:

$$NE\Delta R = \frac{\Delta E \cdot \bar{R}}{\left(\frac{1-\phi}{4f\#^2}\right) T_I \int_{\lambda_1}^{\lambda_2} \bar{W}_S(\lambda) T_O(\lambda) S(\lambda) MTF_S(\nu, \lambda) d\lambda}$$

Where:

$\Delta E$  = Noise equivalent exposure

$\bar{R}$  = Average scene reflectance

$\phi$  = Obstruction ratio

$f\#$  = Optical  $f$ -number,  $\left(\frac{F}{D}\right)$

$T_I$  = Integration time

$\bar{W}_S(\lambda)$  = Average spectral radiant emittance corresponding to the average scene reflectance (without haze)

$T_O(\lambda)$  = Spectral transmittance of the optics

$S(\lambda)$  = Spectral responsivity of the detector

$MTF_S(\nu, \lambda)$  = System modulation transfer functions

$\lambda$  = Wavelength ( $\mu$ )

$\nu$  = Spatial frequency (cycles/mm)



2. Short Wavelength Infrared:

$$NE\Delta R = \left(\frac{\Delta f}{A_s}\right)^{\frac{1}{2}} \frac{\bar{R}}{D^*_{\lambda_p} \left(\frac{1-\phi}{4f\#^2}\right) \int_{\lambda_1}^{\lambda_2} \bar{W}(\lambda) T_o(\lambda) S_N(\lambda) MTF_S(\nu, \lambda) d\lambda}$$

Where:

 $A_s$  = Sensor area $\Delta f$  = Noise equivalent bandwidth $f\#$  = Optical  $f$ -number,  $\left(\frac{F}{D}\right)$  $\phi$  = Obstruction ratio $D^*_{\lambda_p}$  = Peak value of  $D^*$  occurring at  $\lambda_p$  $S_N(\lambda)$  = Peak normalized sensor responsivity $MTF_S(\nu, \lambda)$  = System modulation transfer function $\bar{W}(\lambda)$  = Average spectral radiant emittance of scene $T_o(\lambda)$  = Spectral transmittance of the optics $\bar{R}$  = Average scene reflectance3. Thermal Infrared:

$$NEDT = \frac{NEI}{DR}$$

Where:

NEI = Noise equivalent irradiance

DR = Differential radiance

NEI can be expressed as:

$$NEI = \left(\frac{\Delta f}{A_s}\right)^{\frac{1}{2}} \frac{1}{D^*_{\lambda_p} (1-\phi)} \frac{\int_{\lambda_1}^{\lambda_2} W_E(\lambda) T_A(\lambda) T_o(\lambda) S_N(\lambda) d\lambda}{\int_{\lambda_1}^{\lambda_2} W_E(\lambda) T_A(\lambda) T_o(\lambda) S_N(\lambda) MTF_S(\nu, \lambda) d\lambda}$$

while DR can be expressed as:

$$DR = \frac{1}{4f\#^2} \int_{\lambda_1}^{\lambda_2} \frac{\partial W_E(\lambda)}{\partial T} T_A(\lambda) T_o(\lambda) S_N(\lambda) d\lambda$$



Where:

$\Delta f$  = Noise equivalent bandwidth

$A_s$  = Sensor area

$T$  = Temperature ( $^{\circ}K$ )

$D^*_{\lambda_p}$  = Peak value of  $D^*$  occurring on  $\lambda_p$

$W_E(\lambda)$  = Radiant emittance of the Earth ( $300^{\circ}K$ )

$T_A(\lambda)$  = Atmospheric transmittance

$T_o(\lambda)$  = Optics transmittance

$S_N(\lambda)$  = Peak normalized sensor responsivity

$MTF_s(\nu, \lambda)$  = System modulation transfer function

$\phi$  = Obstruction ratio

$f\#$  = Optical  $f$ -number  $\left(\frac{F}{D}\right)$

The scene characteristics to be entered in these equations can be estimated from available data on earth surface spectral irradiance. The following conditions were assumed for the purposes of this study:

Local time	10:00 a.m.
Latitude	$40^{\circ}$
Season	Equinox
Solar elevation	$41^{\circ}$
Line of sight	Vertical
Average reflectance	12.5% (neutral)
Atmospheric Transmission	74% at .55 micrometers (clean air, urban industrial area)

The irradiance at the satellite for these conditions in watts/m<sup>2</sup> is given in Table 3.1.1-1.

The irradiance at the satellite in the thermal infrared band is a function of the apparent Earth temperature as seen through the atmosphere. Assuming an Earth temperature range of  $260^{\circ}K$  ( $10^{\circ}F$ ) to  $320^{\circ}K$  ( $117^{\circ}F$ ), the irradiance at the satellite in the thermal infrared band ranges from about 24 to 65 watts/meter<sup>2</sup>.

		WATTS/METER <sup>2</sup>		
BAND	SPECTRAL BAND (MICROMETERS)	DIRECT	HAZE	TOTAL
1	.35 - .5	9.4	21.8	31.2
2	.5 - .62	10.7	7.6	18.3
3	.62 - .7	7.1	2.8	9.9
4	.74 - 1.0	14.8	3.2	18.0
5	1.55 - 1.75*	4.33	--	4.33
6	2.10 - 2.40*	2.98	--	2.98

\*Values derived from Infrared Handbook Table 3.18.



### 3.1.2 Selection of Parameters

Many of the parameters of the imaging systems were set by the requirements, constraints, and assumptions discussed in Section 2.0. These include focal length and integration time (set by orbital parameters, detector sizes, and IFOV requirements) and the spectral transmittance of each band (set by the customer requirements). The remaining principal parameters were telescope aperture and detector responsivity or detectivity which normally could be traded off. Optical field requirements, however, dictated selection of a rather fast optical system to control central obstruction; therefore, detector responsivity was the only parameter left for selection. Section 3.2 discusses the candidate optical systems and Section 3.3 discusses detector candidates.

## 3.2 SELECTION OF OPTICS

Compared to the current Landsat scanning systems, a "pushbroom" linear array uses a very wide optical field. At the beginning of the study, the following general approaches were considered:

- a. A single, wide field optical system covering all seven bands.
- b. Two optical systems, one covering the visible and short wavelength infrared bands, and the other covering the thermal infrared band only.
- c. Two optical systems, one covering only the four visible bands, and one covering all of the infrared bands.
- d. Three optical systems, one for visible light, one for the short wavelength infrared, and one for the thermal infrared.

Because of the need for wide spectral response, approach (a) is limited to catoptric (all reflecting) lens types. Approaches (b) and (c) could have a catadioptric (combined refractive/reflective) lens for at least one of the telescopes. In approach (d) all of the telescopes could be catadioptric, if required.

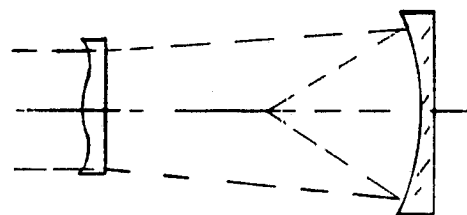


In the study, a survey was made of both types of wide field optical systems, extending previous optical design studies at Kodak and drawing from DOD- and NASA-funded studies at other industries. Candidate optical systems were compared against the following criteria:

1. Spot size over the focal area
2. Manufacturability and testability (number and severity of aspheric surfaces, tolerances, symmetry, etc.)
3. Spectral bandwidth (number and type of refractive elements)
4. Size of components and size of assembly
5. Stray light suppression
6. Estimated development schedule

### 3.2.1 Catadioptric Lens Configurations

The best known and most widely used catadioptric lens is the classical Schmidt design. An aspheric corrector plate located at the center of curvature of the spherical primary mirror produces exceptionally high image quality, over a wide field-of-view (FOV) at small to moderate  $f$ -numbers, on a curved image surface (see Figure 3.2.1-1). With solid state sensors, a stigmatic curved field is easily accommodated. For a broad spectral band optical system, this design requires a transmitting material which can cover the spectral region of interest. The dispersion characteristics must also be low; if they are not, individual focusing may be required for each band, especially at the short wavelengths. In this



TRANSMITTING SCHMIDT

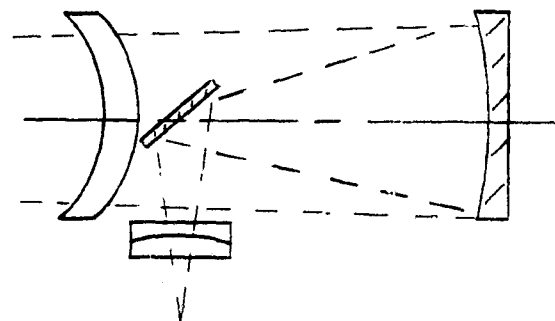
Figure 3.2.1-1

region, the dispersion will probably be high, as will the image quality requirements. Central obstruction is a serious problem. The detectors and associated equipment will have to be located for easy access. A flat mirror and a pierced primary would yield the largest central obstruction and can, therefore, be eliminated from further consideration. A much smaller obstruction is obtained with a long, narrow reflex mirror which redirects the

image forming rays to the side; alternately, an equivalent obstruction would be obtained with a folding flat mirror. A long, narrow slot in this mirror would pass the image after reflections from the flat mirror and the spherical mirror, respectively. To cover a long, very narrow FOV, such as the 0.35 - 1.0 micron detectors, the resulting bar obstruction in either case would be quite acceptable. If the in-track FOV is increased to accommodate an additional spectral band (1.5 - 2.4 microns), however, the necessary obstruction width would increase significantly with image quality deteriorating due to diffraction effects.

Meniscus corrector optical systems are frequently a viable alternative to the classical Schmidt. In this instance, spherical aberration correction is achieved with spherical surfaces. The monocentric version, commonly called the Bouwers design, is capable of a wide FOV over a curved image surface free from coma and astigmatism in a manner similar to the Schmidt. Since the spherical aberration of this design is corrected by the meniscus thickness, a design which meets the image requirements of this program in the 0.35 - 1.0 micron region would require a thick, heavy corrector lens. The obstruction characteristics of the Bouwers are the same as those of the Schmidt.

The Maksutov meniscus corrector design (see Figure 3.2.1-2) is achromatic. By virtue of the meniscus corrector lens shape and power, spherical aberration and longitudinal color are corrected; the Maksutov design can easily accommodate the spectral region from 0.35 - 1.0 micron due to its inherently low spherochromatism residual. The Maksutov design is not



MAKSUTOV

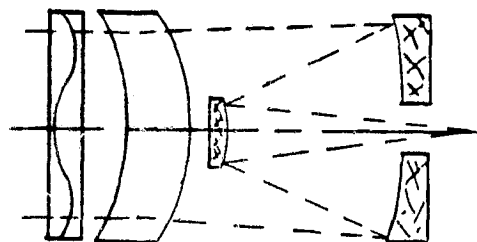
Figure 3.2.1-2

monocentric. Since the corrector is located approximately one focal length in front of the primary mirror and the corrector-spherical mirror radii centers are not coincident, there is an astigmatism residual on a curved image surface which requires field lenses near the image surface for correction. Lateral color would preclude a single field lens design over the 0.35 - 1.0 micron spectral region, resulting in a multiple field lens array to accommodate this

band. Separate field lenses, in conjunction with beam splitters, would be able to cover the four bands if sufficient back focus could be achieved. However, this approach would probably significantly reduce the FOV. To cover two spectral regions, 0.35 - 1.0 micron and 1.5 - 2.5 microns (assuming that the field lens problem could be solved), would degrade the obstruction characteristics which would be the same as the designs previously discussed when in-track FOV is increased.

The Schmidt-Cassegrain and Schmidt-Maksutov Cassegrain have been utilized in other space programs which required a more restricted FOV or spectral bandwidth. Figure 3.2.1-3 is a basic configuration of this type. These designs

have two advantages: field aberration correction is accomplished with mirrors so that the problems which afflict the Maksutov design are eliminated, and spherical aberration and axial color are corrected with a meniscus corrector lens and a multiple asphere doublet Schmidt-type corrector. However, the meniscus is thick, the two Cassegrain mirrors are aspheric, and there is a very large central obstruction in covering a 15-degree FOV. Though capable of overcoming some of the shortcomings of the previous configuration, this design would be impractical to build.



*SCHMIDT-MENISCUS CASSEGRAIN*

*Figure 3.2.1-3*

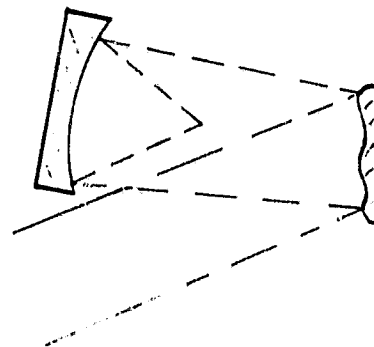
In summary, none of the catadioptric forms appear capable of covering the required field at the required image quality over the first six bands in a practical, manufacturable design.

### 3.2.2 Catoptric Lens Configurations

Catoptric (all reflecting) optical systems have no chromatic aberrations and can, therefore, be used over broad spectral bands. A single catoptric system could, in principle, be used for all three spectral regions. The Defense Advanced Research Projects Agency (DARPA) and NASA have recently sponsored a great deal of investigation of catoptric optical forms for use on projects such as HALO and large, broadband space telescopes. Only three approaches

have been identified which provide wide field coverage and good optical performance: the reflecting Schmidt, the Walrus\*, and the inverse Schwarzschild.

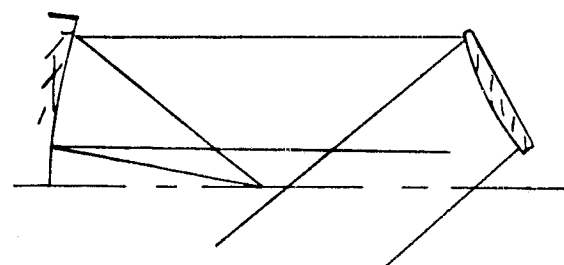
The reflecting Schmidt is the smallest and simplest of these designs (see Figure 3.2.2-1). In the reflecting Schmidt the transmitting aspheric corrector is replaced with the reflecting equivalent. Since in the axially symmetric mode the design would be 100 percent obscured, the reflecting corrector has to be inclined to the optical axis to avoid the obscuring effects of the primary mirror. If the mirror tilt can be kept moderate (12 degrees) and the relative aperture can be limited to about  $f/4$ , the reflecting corrector figure can be symmetric, simplifying manufacturing and testing. If both of these parameters are significantly increased, a toroidal asphere (commonly referred to as the "potato chip shape") would be required which would increase the difficulty to fabricate and test the mirror. Utilization of an off-axis reflecting Schmidt for multiple-band spectral coverage will, unfortunately, still be limited by obstruction effects when the in-track FOV is increased to accommodate the additional spectral regions. Obstruction effects would be quite large, even with beam splitters, because of the long mechanical back focus required.



REFLECTING SCHMIDT

Figure 3.2.2-1

There is an unobstructed version of the reflecting Schmidt (see Figure 3.2.2-2), but this configuration would put a heavy burden on correction of spherical aberration since a relative aperture at least twice as fast as the nominal aperture is required. To truly be unobstructed and have an accessible image surface,  $f/1.75$  would be needed.



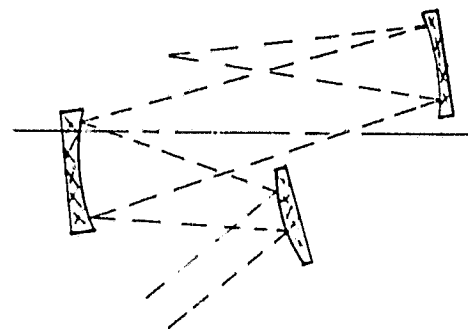
REFLECTING SCHMIDT UNOBSTRUCTED

Figure 3.2.2-2

\*Walrus--An acronym for Wide Angle Large Reflecting Unobstructed System.

This approach would definitely require a toroidal asphere, which would certainly offer problems in manufacture, test, and alignment of the off-axis segment.

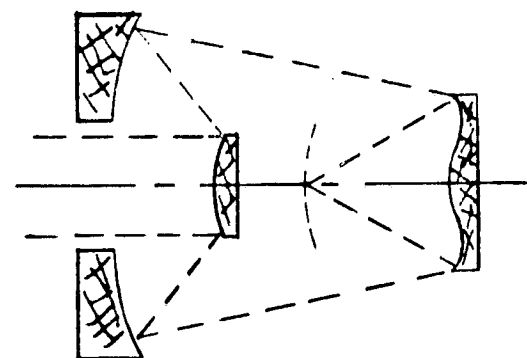
Another unobscured catoptric configuration which would meet the performance requirements of this program in all three spectral regions is the Walrus design (see Figure 3.2.2-3). This configuration is a reflecting version of the classical retro-focus lens. By using three aspheric mirrors off-axis, excellent image quality can be achieved over a wide field of view at moderate  $f$ -numbers. This design is long relative to its focal length and can be quite large, and fabrication, testing, and alignment of the three off-axis aspheric segments can pose difficult problems.



WALRUS

Figure 3.2.2-3

A more promising catoptric design is the inverse Schwarzschild, which is basically a Cassegrain that is used backwards (see Figure 3.2.2-4). This design differs from the Cassegrain in that the centers of curvature of the spherical mirrors are coincident. By proper choice of radii the system is corrected for third order spherical and all oblique aberrations. The very wide field of view is imaged on a curved image surface whose center of curvature is coincident with the tertiary. If a mild aspheric figure is put on a plano mirror which is located at the center of curvature of the mirrors, the image quality is significantly improved.



INVERSE SCHWARZSCHILD

Figure 3.2.2-4

The secondary mirror is necessarily large because of the convex primary. The minimum secondary mirror diameter is achieved by locating the stop at the secondary mirror. To keep the obstruction ratio to a manageable level requires that the system  $f$ -number be about  $f/2.5$ , resulting in a ratio of primary to secondary mirror diameter of about 3 to 1.



The inverse Schwarzschild was selected as our baseline design for the principal optical telescope because this design meets the image requirements of the program and can accommodate all three spectral regions. It is a very simple design consisting of two spheres and a very weak aspheric plano mirror (about 1.5 waves asphericity), and is basically a very low risk optical configuration.

### 3.2.3 Thermal IR Optical Telescope

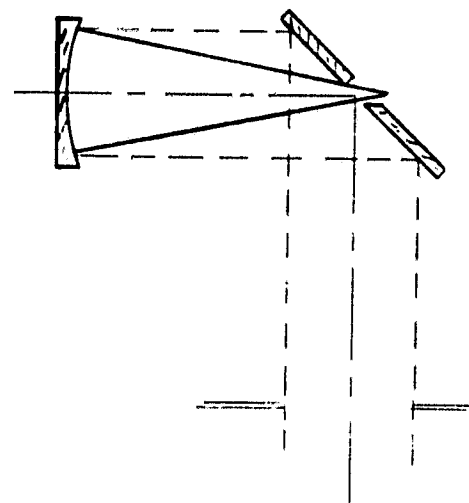
The baseline Schwarzschild design can easily accommodate the three spectral regions, assuming that all detectors and optical bay areas would be at the same temperature to avoid the need for cooling apparatus, cold baffles, etc. Unfortunately, thermal IR detectors have to be operated at low temperatures and the cooling apparatus is of appreciable size. Since location of the space radiator on a stationary, cold surface of the spacecraft is very desirable (as discussed in Section 2.1.2), we decided to locate the thermal IR optics in a separate bay.

Since the spectral region covered is from 10.5 - 12.5 microns and the detector size is 100 microns by 100 microns, the image requirements are significantly reduced compared to those for the other spectral regions. With less stringent requirements, a very simple optical system can be employed. The configuration selected could be considered a "lens-less Schmidt", that is, a spherical mirror with the aperture stop at the center of curvature. This arrangement will produce a FOV of uniform image quality over a curved image surface. Radiometric calculations indicated that an  $f/5$  system would be satisfactory, yielding a geometrical spot size for 80 percent of the image encircled energy of about 45 microns and a diffraction spot size of about 100 microns.

Obstruction problems which were discussed earlier (the Schmidt design, for instance), can be better handled in the thermal IR design. Figure 3.2.3-1 shows the basic configuration. To obtain sufficient mechanical back focus for cold shielding, clearance for the cooling apparatus, etc., the pierced folding mirror has to be moved toward the primary mirror. When the detector array has been properly located, the resulting bar obstruction will obscure about 25 percent of the area of the entrance pupil. The lens has to cover a FOV of 15 degrees



in the cross-track direction and a fraction of a degree in the in-track direction. By comparison, the inverse Schwarzschild can cover a circular 15 degree FOV with a 50 percent entrance pupil area obstruction. If desired, the bar obstruction area effects could be compensated by making the system relative aperture about  $f/4.5$ , which would still provide a spot size compatible with the system requirements.



BASIC FOLDED "LENSLESS" SCHMIDT  
CONCEPT FOR THERMAL TELESCOPE

Figure 3.2.3-1

For this spectral region we have identified a diffraction-limited optical system with the simplest of optical elements. To locate the image surface at the desired spacecraft location and to make it accessible, two flat folding mirrors have been embodied into the optical system. Because of the detector placement, these mirrors locate the thermal infrared FOV parallel to that of the principal telescope, though separated axially.

### 3.3 SELECTION OF DETECTORS

The "pushbroom" concept employs a linear array of detectors for each spectral band. A brief survey of suppliers was made, consistent with the study goal of using only near-term technology, to establish the characteristics of visible and infrared detector arrays that might be used in the 1983 to 1985 time period. The following sections discuss the requirements for detectors in each spectral band and present the results of each survey. A baseline detector array configuration is selected for each spectral region.

#### 3.3.1 Detector Arrays for the Visible Bands

The requirements for resolution (10-meter FOV) and swath coverage (185 km) dictate that each visible band have a linear array of 18,500 contiguous detectors. To implement the four "visible" bands in a single focal plane with

good pixel-to-pixel registration between bands, it is highly desirable to have all four bands on each chip. Other detector characteristics of interest are the quantum efficiency in each band, detector physical/electrical uniformity and temporal/thermal stability, and the anticipated development time for the detector array.

The only two types of detectors considered were silicon photodiode arrays and silicon charge coupled detector (CCD) arrays. The CCD arrays are clearly advantageous for low light applications because they permit operation in a time delay and integration (TDI) mode wherein an image moves sequentially across multiple rows of detectors which are clocked at a rate commensurate with the image motion. This mode gives the advantage of an extended integration time without the disadvantage of increased smear. For the conditions of this study, however, operation in the TDI mode is not particularly advantageous because a fast lens is required for optical field reasons anyway. The choice between photodiode arrays and CCD arrays can therefore be made on a technology/schedule basis later in the program.

Most of the information on silicon detector arrays was obtained from meetings and telecons with personnel at the Westinghouse Defense and Electronics Systems Center in Baltimore, Maryland. These discussions confirmed that the required detector arrays will be within the state-of-the-art in the 1983 to 1985 time period. The baseline detector array configuration that resulted from these discussions is presented in Section 4.2.

### 3.3.2 Detector Arrays for the Short Wavelength Infrared Bands

Selection of a baseline detector for the two short wavelength infrared (SWIR) bands was more difficult than for the visible bands because more detector materials are available and because performance is a function of temperature as well as material. The basic requirements for these detectors are to provide an IFOV of 20 meters or better and a sensitivity to changes in reflectivity of 1.0 percent for Band 5 and 2.4 percent for Band 6. For a one-meter focal



length (corresponding to a 10-meter IFOV in Bands 1 through 4), the SWIR detectors must be 30 microns or less in width. The required D Star for these bands, as shown in Figure 3.3.2-1, is about  $8 \times 10^9$  for Band 5 and about  $5 \times 10^9$  for Band 6. Detectors for this case are:

Photoconductive

PbS at 195<sup>0</sup>K to 295<sup>0</sup>K

InAs at 77<sup>0</sup>K

InSb at 77<sup>0</sup>K

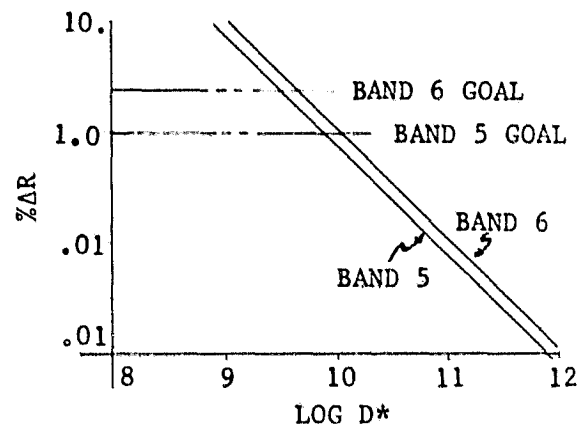
HgCdTe at 250<sup>0</sup>K

Photovoltaic

HgCdTe at 195<sup>0</sup>K

InAs at 77<sup>0</sup>K

Companies visited to obtain data on SWIR cells included Honeywell Electro-Optics Center, Westinghouse, and Aerojet General. Other contacts included Santa Barbara Research Center, Texas Instruments, RCA, Rockwell, and ITT.



PERCENT DELTA REFLECTANCE  
VERSUS  
D-STAR

Figure 3.3.2-1

As discussed in Section 3.1, the SWIR detectors share the focal plane of the principal telescope with the visible detectors. It is therefore desirable to select cells which can operate at temperatures reasonably close to that of the principal telescope enclosure. Operation in the photovoltaic mode (at zero bias) was also considered desirable to avoid the use of a chopper, which could be a reliability issue for long missions. These reasons led to the selection of HgCdTe, operating in the photovoltaic mode at 195<sup>0</sup>K, as the baseline SWIR detector choice. This selection appears to be reasonably low in risk because similar detectors are being developed for several other applications. The physical configuration of the selected detector array is discussed in Section 4.2.

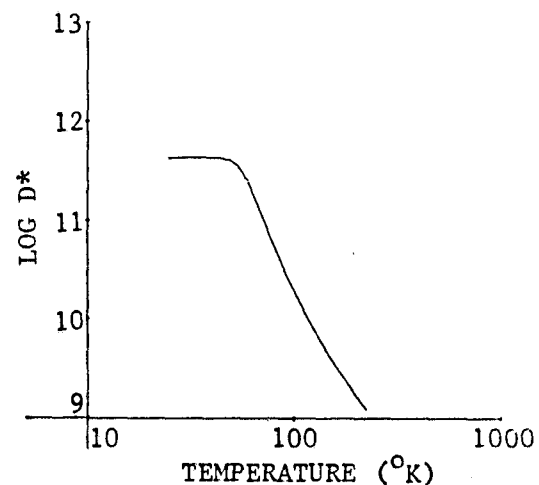
### 3.3.3 Detector Arrays for the Thermal Infrared Band

The detectors in the thermal infrared channel measure temperature differences on the Earth's surface. The basic requirement for these detectors is to provide a sensitivity to changes in temperature of 0.5<sup>0</sup>K or better. Detector

size and system IFOV were not specified by NASA for this study. On a parallel procurement, however, NASA-Goddard Space Flight Center (GSFC) has requested proposals for development of a 1000-element array of 100 by 100 micrometer thermal infrared detectors, with a detectivity ( $D^*$ ) of  $1.5 \times 10^{10}$   $\text{cmHz}^{1/2}/\text{w}$  at  $105^\circ\text{K}$ . These requirements were used as the basis for the thermal infrared detector survey. (For the assumed system parameters, three such 1000-element arrays would be required.)

Detectors for the thermal infrared band were discussed with Westinghouse and Honeywell, and with Dr. T. J. Treadwell of the Kodak Research Laboratories. Although considerable effort had previously gone into developing lead-tin-telluride detectors, mercury-cadmium-telluride (HgCdTe) appears to be the only type of detector now in active development.

Selection of operating temperature was a more difficult choice than selection of detector type. Detectivity of thermal photocells increases with decreasing temperature (see Figure 3.3.3-1). The size and sophistication of the thermal control system also increases with decreasing temperature. In relation to the design objective of passive cooling, operating temperature must be sufficiently high to allow radiation to outer space of heat absorbed into and generated within the detector assembly. Tradeoff studies between sensitivity and cooling requirements have led to a compromise at  $105^\circ\text{K}$  as a suitable operating temperature. The physical configuration of the baseline thermal detector arrays is discussed in Section 4.2.



*D-STAR VERSUS TEMPERATURE  
TIR DETECTORS*

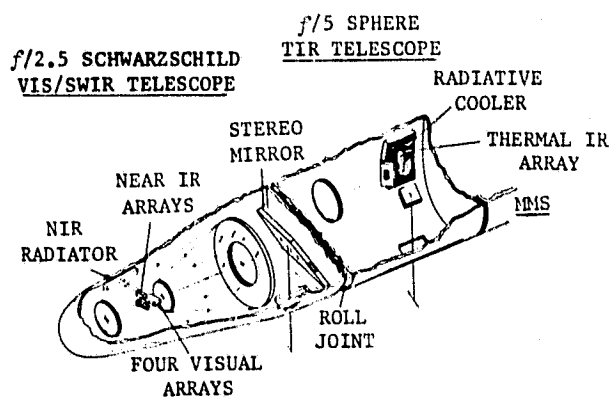
*Figure 3.3.3-1*



### 3.4 CONFIGURATIONS

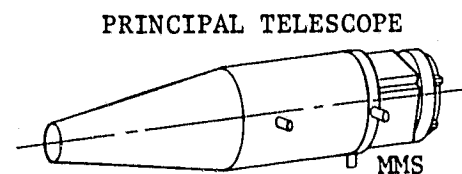
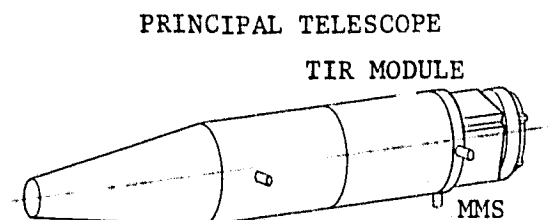
Early in this study several decisions were made which affected the selection of a configuration concept. As discussed in Section 2.1.2, use of a compensated "roll joint" for roll pointing and a plano mirror for stereo pointing appeared to offer the best combination of pointing characteristics for the visible and short wavelength infrared (SWIR) sensors. To provide passive, radiative cooling of the thermal infrared sensor requires access to a large area of the spacecraft surface with a good, constant view factor of cold space. It was decided that the thermal infrared sensor should be a separate instrument mounted on the fixed spacecraft structure.

These decisions led to the selection of the general spacecraft configuration shown in Figure 3.4-1. In this approach, the visible and SWIR sensors share a Schwarzschild telescope (designated the principal telescope) and the thermal telescope is separately mounted as a module to the spacecraft structure. The thermal telescope and principal telescope can be operated completely independently; however, provision will be made for boresighting the thermal telescope line-of-sight to the zero roll, zero stereo line-of-sight of the principal telescope. If development of the thermal telescope is delayed, the principal telescope could be mounted directly to the MMS as shown in Figure 3.4-2.



GENERAL SPACECRAFT CONFIGURATION  
APPROACH

Figure 3.4-1



ALTERNATE CONFIGURATIONS

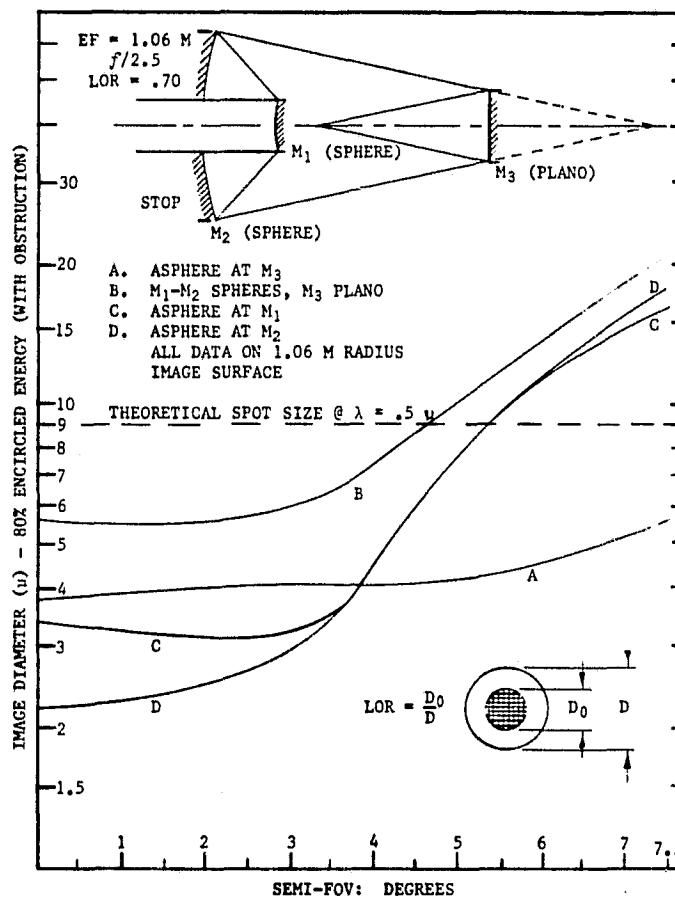
Figure 3.4-2

#### 4.0 DESIGN APPROACH FOR THE PRINCIPAL TELESCOPE

The selected design approach for the principal telescope is described in this section. The principal telescope is comprised of an outer shell, a metering and support structure, the Schwarzschild optics, the visible and SWIR detector arrays, and the associated electronic and thermal control components. The following subsections describe these components and present estimated performance characteristics of the telescope.

#### 4.1 OPTICS

The baseline Schwarzschild telescope is comprised of a convex primary mirror, a large concave secondary mirror, and a plano folding mirror (see Figure 4.1-1).

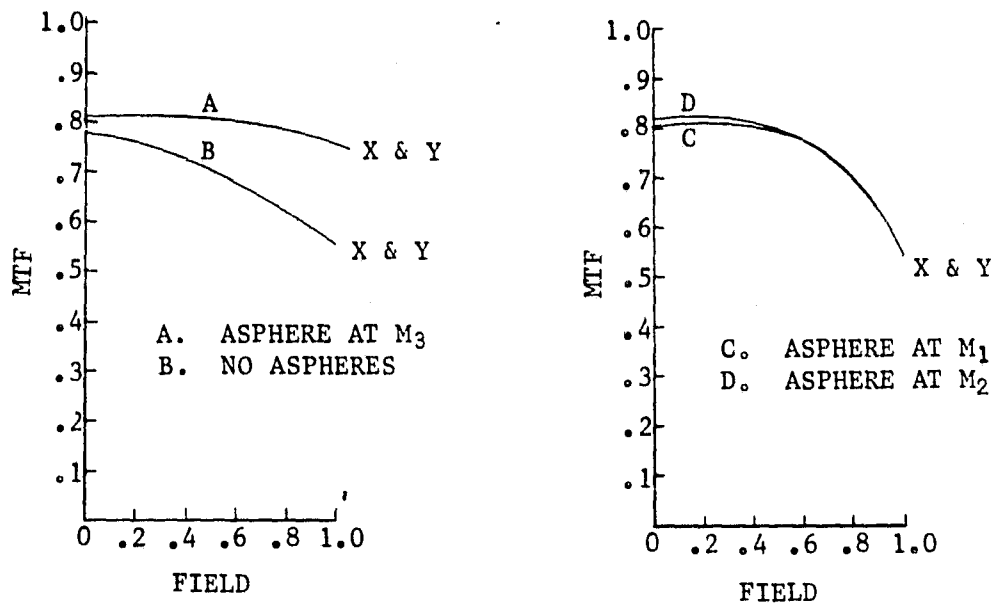


PRINCIPAL TELESCOPE OPTICS

Figure 4.1-1

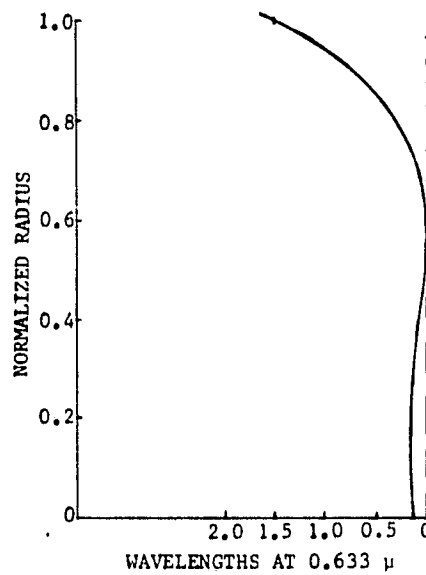


The secondary mirror size is minimized if the field stop is placed at the secondary mirror. Reasonably good image quality over a wide field can be achieved if the curved mirrors are concentric spheres and the plano has no aspheric correction. The on-axis image quality is improved by aspherizing either of the spheres. Performance off-axis is best if the aspheric correction is applied to the plano. Spot sizes and MTF's associated with these options are shown in Figures 4.1-1 and 4.1-2. For the study baseline, the aspheric surface was applied to the plano. This weak asphere is shown in Figure 4.1-3. The nominal physical and optical characteristics are shown in Figure 4.1-4.



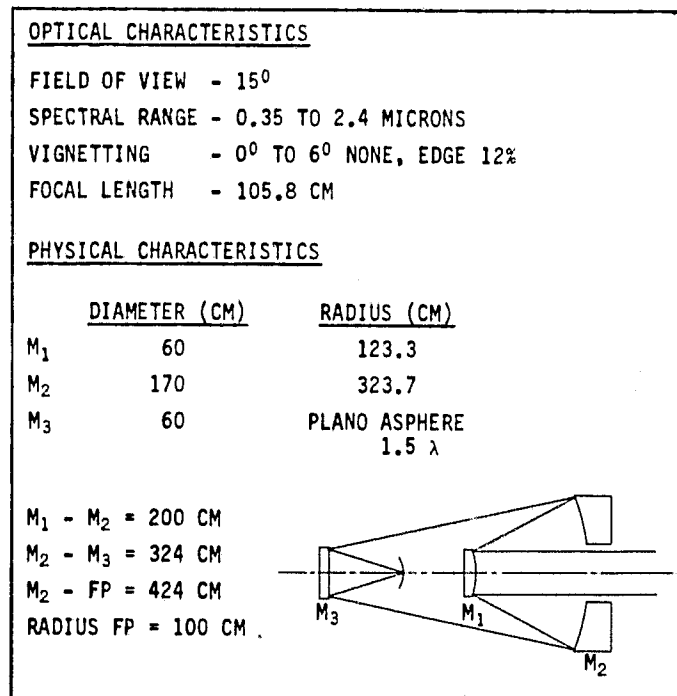
INVERSE SCHWARZSCHILD MTF DATA AT 33 L/MM AND 500 nm  
 X = IN-TRACK      Y = CROSS TRACK

Figure 4.1-2



SCHWARZSCHILD ASPHERIC TERTIARY MIRROR

Figure 4.1-3



PHYSICAL AND OPTICAL CHARACTERISTICS  
OF THE PRINCIPAL TELESCOPE

Figure 4.1-4

#### 4.1.1 Optical Sensitivities

The optical sensitivities for the principal optical telescope (listed in Table 4.1.1-1) were determined by perturbing all the parameters to produce the same effect. The aspheric tertiary mirror located at the center of curvature for both the spherical mirrors and detector array can be tilted about its vertex without introducing any focus errors; it merely shifts the line of sight. The tertiary is very insensitive to decentering; therefore, these sensitivities effect a control on image location rather than affecting focus errors. Since the outer portions of the optics mainly affect higher spatial frequencies, the surface figure (aspheric departure) was modeled by adding a y-fourth term which reflects the lower frequency domain at which the telescope will function.

<i>Table 4.1.1-1</i> PRINCIPAL OPTICAL TELESCOPE SENSITIVITIES	
PRIMARY MIRROR	<ul style="list-style-type: none"> <li>● RADIUS = <math>\pm 2.0</math> MM WITH REFOCUSING AND READJUSTMENT OF AIRSPACE BETWEEN PRIMARY AND SECONDARY MIRROR</li> <li>● AIRSPACE = <math>\pm 1.0</math> MM WITH REFOCUSING</li> <li>● DECENTER = <math>\pm 0.075</math> MM, HORIZONTAL AND VERTICAL</li> <li>● TILT = <math>\pm 15.0</math> SECONDS, HORIZONTAL AND VERTICAL</li> <li>● SURFACE FIGURE = .4 WAVE ASPHERIC DEPARTURE OVER THE CLEAR APERTURE (.08 WAVE RMS SURFACE QUALITY)</li> </ul>
SECONDARY MIRROR	<ul style="list-style-type: none"> <li>● RADIUS = <math>\pm 2.0</math> MM WITH REFOCUSING AND READJUSTMENT OF AIRSPACE BETWEEN PRIMARY AND SECONDARY MIRROR</li> <li>● AIRSPACE = <math>\pm 2.0</math> MM WITH REFOCUSING</li> <li>● DECENTER = <math>\pm .05</math> MM VERTICAL; <math>\pm .10</math> MM HORIZONTAL</li> <li>● TILT = <math>\pm 5.0</math> SECONDS, HORIZONTAL AND VERTICAL</li> <li>● SURFACE FIGURE = .4 WAVE ASPHERIC DEPARTURE OVER THE CLEAR APERTURE (.08 WAVE RMS SURFACE QUALITY)</li> </ul>
TERTIARY MIRROR	<ul style="list-style-type: none"> <li>● RADIUS = <math>\pm 300</math> RINGS OVER THE CLEAR APERTURE (<math>\lambda = 6328 \text{ \AA}</math>)</li> <li>● AIRSPACE = IMAGE FOCUS SETTING; <math>\pm .01</math> MM</li> <li>● DECENTER = <math>\pm .10</math> MM, HORIZONTAL AND VERTICAL</li> <li>● TILT = <math>\pm 30.0</math> SECONDS, HORIZONTAL AND VERTICAL</li> <li>● SURFACE FIGURE = .4 WAVE ASPHERIC DEPARTURE OVER THE CLEAR APERTURE (.08 WAVE RMS SURFACE QUALITY)</li> </ul>



The perturbations reflect a change in the design MTF at 33 L/mm of 0.02 from the nominal of 0.81. Statistical analysis of these sensitivities as  $3\sigma$  limits predicts a manufactured system which will be no worse in MTF than 92 percent of the design value. This compares to a resulting system rms wavefront error of 0.075 wave. All of the sensitivities are well within the range of normal manufacturing and testing controls. No high risk tolerances have been identified.

The principal optical telescope operating temperature in the main bay will be 250°K, which is a 44°K drop from the nominal room temperature testing environment. Assuming ULE mirrors and an invar structure, the resulting increase in back focus is 0.2699 mm; therefore, after final assembly and testing, the telescope will have to be readjusted to be in focus at the orbital operating temperature.

#### 4.1.2 Calibration

To reconstruct an image without streaking and with a known radiometric relationship among the pixels, it is necessary to define the relative calibration of each element in the array. This calibration is obtained by determining the slope and intercept (transfer characteristic) for each element.

A second problem is to determine the absolute reflectance of the ground scene if the transfer characteristic of each detector is known. Absolute reflectance determination will not be discussed in this report.

In order to effect relative calibration, it is necessary to introduce a uniform source of light to the image plane. It must have the following features:

1. Controllable intensity at several levels.
2. Known spectral distribution.
3. Known distribution with field angle.

Other desired features include:

1. Measurement through the entire optical imaging chain.
2. Low probability of the source failing either *ON* or *OFF*.



3. Easy activation with a minimum expenditure of vehicle power.
4. Calibration at any time in the mission.

It is attractive to consider the use of a celestial object as the light source. Since stars or planets are too small and too dim and the moon is not always available as a bright object, the sun is the only candidate. To direct the sun to the image plane, either the entire vehicle must be pointed at the sun or a special pointable, sun-collecting telescope is required. Pointing the entire vehicle is probably the best way of effecting calibration of the entire imaging chain. It is estimated, however, that the changes in optical transmittance over the life of the mission will be slight, whereas it is certain that vehicle pointing will require a lengthy period to accomplish with a concomitant heavy use of vehicle power and a long post-calibrating settling time; thus, it was decided to consider only a pointable, sun-collecting telescope.

The sun is available on the day side of the orbit. If it is desirable to calibrate at any time during the daylight pass, the satellite must be fitted with commandable light-tight doors to block scene radiation. It is possible, however, to capture the sun for a short period when the satellite is crossing the terminator, but when the line-of-sight views a dark scene. In this case, it may be possible to eliminate the need for doors, which are a reliability hazard.

Complicating this calibration is a small, long-term variation in the solar output. This fluctuation, however, is within the requirement for radiometric accuracy.

In summary, the sun as a calibration light source is advantageous because it is a never-failing source of a high brightness and color temperature. Disadvantages are that either the satellite must be supplied with doors (which are a reliability hazard) to permit daylight calibration, or calibration must be restricted to a rather narrow time window at the poles. This approach requires a pointable sun telescope.



Another method of obtaining calibration is to employ an internal, artificial light source. The source must have a high color temperature sufficient to supply an output in the range from Band 1 to Band 6, and a spectral output without absorption lines or spectral peaks. Tungsten-halogen bulbs meet these requirements. For example, the 6-volt, 12-watt, Sylvania ERA bulb has a color temperature of 3350<sup>0</sup>K at rated voltage. The output in Band 1 will be about 15 percent of the peak value and in Band 6, about 25 percent of the peak value. If the lamp is operated at 83 percent of rated voltage, the light output will drop to 56 percent, and the color temperature will decrease to 3120<sup>0</sup>K, but the life will increase by a factor of ten. The advantage of an internal, artificial source is that it may be used for calibration at any time on the dark side of the orbit, thus eliminating the need for operating doors. It is also unnecessary to have a pointable telescope or to require a special vehicle attitude. The disadvantage is that the bulbs have a limited life. Assuming a calibration procedure which lasts four to five seconds, twice per revolution, a bulb would acquire about 40 hours of use over a three-year life span. Assuming some factory use and a reasonable factor-of-safety, bulbs with 100 to 200 hours rated life are required. If the bulbs are operated at somewhat less than rated voltage, the life can be extended by a large factor.

It was assumed that calibration twice per revolution would be desirable. There are indications, however, that this frequency is considerably in excess of what is required. Perhaps calibration as seldom as every few days will be sufficient, particularly if the temperature of the image plane is well-controlled. In an existing application, the image plane is controlled to about  $\pm 2.0^{\circ}\text{C}$ , whereas control to  $\pm 0.2^{\circ}\text{C}$  is planned for this program. As a result, the usage of the bulbs would be much less than was initially assumed, easing the requirements for bulb lifetime.

A brief survey of manufacturers' literature indicates that suitable, miniature tungsten-halogen lamps are available. By monitoring the current and voltage to the lamp, the intensity can be predicted to within a few percent, which is within the requirements for radiometric accuracy.

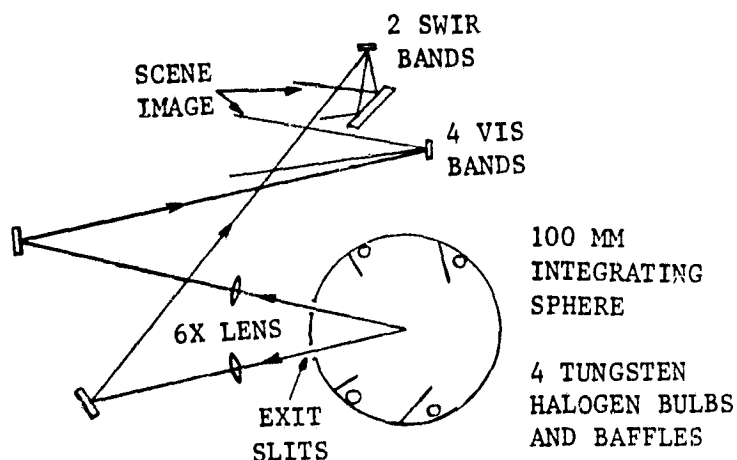


After a review of the advantages and disadvantages, a tungsten-halogen lamp was selected in preference to the sun for a calibration source. The reliability hazard of premature bulb failure seemed to be worth the risk compared with the inconvenience of attempting to use the sun and the reliability hazard of a pointing telescope.

Regardless of whether the sun or a tungsten-halogen source is used, a uniform (or at least known) strip of light must be directed to the image plane. To illuminate the entire array, the light strip must be about 11 inches long and a fraction of an inch wide. The intensity must be uniform to about 0.1 percent. It was decided that a diffuse (rather than specular) source would give the most uniform output. Several schemes were investigated, including a diffusing screen, a tunnel or conical diffuser, and an integrating sphere. The integrating sphere was selected, since it offered the most uniform light source.

As a rule of thumb, an integrating sphere may have no more than 5 percent of the surface area taken up with ports if the output is to be uniform and diffuse. Assume a 100-mm diameter sphere. If four, 10-mm diameter lamps are employed and two 1-mm by 50-mm exit ports are required, the port area is only 4 percent of the surface area. Using four lamps of different wattages, sixteen different intensity levels can be generated. Four lamps also provide a measure of redundancy, protecting against premature lamp failure. Two exit ports are required because the visual bands and the near IR bands are physically separated at the image plane. Projector telescopes are used to transfer enlarged images of the exit ports to the sensors. A magnification of about six is required. Because these telescopes will exhibit approximately cosine-cubed fall-off with field angle, the slit of light at the sensors will have this function (yielding about 90 percent of the axial value at the edge of the field). However, the intensity fall-off will be a gentle, well-behaved function which will be invariant with time, and calibrated in the factory. An optical schematic of this calibration scheme is shown in Figure 4.1.2-1.





CALIBRATION DEVICE FOR VIS/SWIR BANDS

Figure 4.1.2-1

## 4.2 DETECTORS

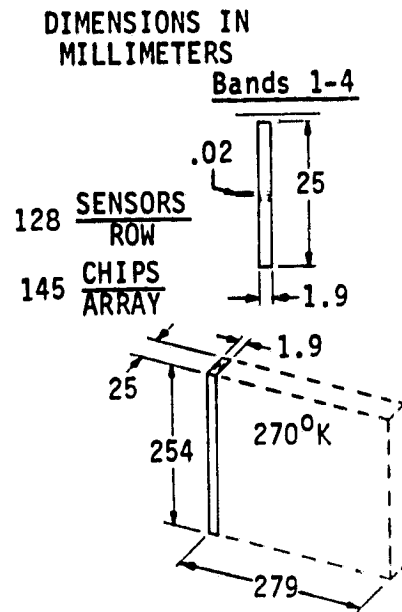
### 4.2.1 Introduction

A brief survey of detector manufacturers was conducted to assess the state-of-the-art in detector arrays capable of satisfying the mission requirements in the 1983 time frame (see Section 3.2). Results of this survey are contained in the following sections, in which baseline detector configurations and characteristics for the first six bands are discussed. The selected baseline for Band 7, the thermal infrared band, is discussed separately in Section 5.2.

### 4.2.2 Detectors for the Visual Bands: Bands 1 - 4

4.2.2.1 Configuration - The baseline detector array for Bands 1 through 4 evolved from discussions with personnel at Westinghouse Defense and Electronics Systems Center in Baltimore, Maryland. The baseline array reflects our study objectives: to minimize the focal plane congestion; to achieve inherent band-to-band geometric registration and radiometric accuracy; and to propose a focal plane array which can be built with confidence in the 1983 time frame. An

array which satisfies these objectives is illustrated in Figure 4.2.2-1. The array is comprised of 145 individual chips or subarrays. Each chip consists of four parallel linear arrays, one for each band. The subarrays are separated by five micrometers in-track and each contains 128 detectors. The focal plane, therefore, consists of four linear arrays, each containing 18,560 detectors. The detectors are silicon CCD's, with an aperture of  $15\mu \times 15\mu$ , on  $15\mu$  centers. To obtain the spectral separation for each band, appropriate multilayer filters are deposited directly on the individual linear arrays.



BASELINE FOCAL PLAN ARRAY  
FOR BANDS 1 - 4

Figure 4.2.2-1

Application of the filters is accomplished by utilizing the original CCD mask to precisely deposit the filter material in the proper location on a chip. The CCD mask is itself masked to allow only the desired array to be coated. This process is repeated until each of the four arrays has been coated with the proper spectral filter.

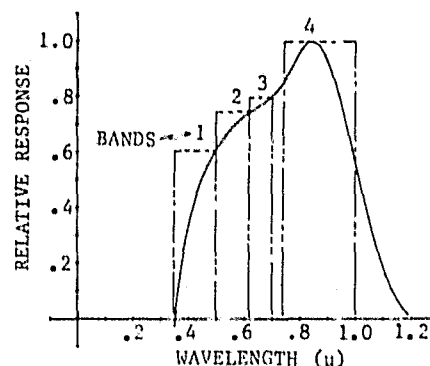
Conversations between Westinghouse and Optoline indicate that it is feasible to obtain filters with an in-band transmittance greater than 80 percent and an out-of-band transmittance of less than 3 percent. The filters, which are constructed from inorganic materials, are well suited to a space environment and should display excellent stability over a temperature range of  $0^{\circ}\text{C}$  to  $70^{\circ}\text{C}$ .

The 11-inch focal plane is constructed by butting together the 145 individual chips. Proper alignment of the chips necessitates precise laser beam trimming of both ends of each chip and, as a consequence, one detector on each end of a chip is destroyed. These dead pixels require the on-board processor or ground reconstruction equipment to supply these missing signals in order to prevent streaking in the ground reconstructed imagery. The missing signals can be supplied through various algorithms, such as estimators or averagers.

Readout of the four arrays is accomplished as follows. The CCD detectors from a given array (i.e., a particular spectral band) parallel transfer their photo-charge to a shift register which is buried beneath the photosites. This register sequentially transfers the signal charge to signal processing electronics and multiplexers which combine these signals with those from other chips. Readout of all four arrays within one integration period may be accomplished in various ways. These include simultaneous (parallel) readout of the four arrays or sequential readout in which the parallel and series charge transfer operations are performed within one fourth the integration period.

The signal processing electronics, which is under the control of the ground station, is located directly behind the image sensors. This volume contains the control circuitry, the signal conditioning, clocking circuitry, and multiplexers. The control circuitry responds to both spacecraft and ground station commands, and provides the necessary control signals for adjusting the integration and readout times, on-chip resistance heaters, multiplexing rates, etc. The control circuitry is also responsible for performing cross-strapping. Cross-strapping adds together signals from adjacent in-track and cross-track sensors to provide an electronically adjustable pixel size. This technique is useful for extending the exposure range and/or reducing the data rate with a concomitant reduction in ground resolved distance (GRD).

**4.2.2.2 Detector Characteristics** - The detectors which comprise the arrays for Bands 1 through 4 are front-side illuminated, buried channel, silicon CCD's with a transparent tin-oxide gate structure. The normalized spectral responsivity for these detectors is shown in Figure 4.2.2-2, with the spectral bandpass for each of the four bands.



RELATIVE SPECTRAL RESPONSIVITY  
OF SILICON CCD'S FOR BANDS 1 - 4

Figure 4.2.2-2

The detector characteristics for this array are listed in Table 4.2.2-1.

<i>Table 4.2.2-1</i> <i>SILICON CCD DETECTOR CHARACTERISTICS</i>	
APERTURE	15 $\mu$ x15 $\mu$
PITCH	15 $\mu$
DIFFUSION LENGTH	$\sim$ 100 $\mu$
DEPLETION WIDTH	1.5 $\mu$ - 2.0 $\mu$
TRANSFER INEFFICIENCY	10 <sup>-4</sup>
RMS DARK NOISE (300 <sup>o</sup> K)	20 - 30 ELECTRONS
DARK CURRENT VARIATIONS	3 TO 1
GAIN VARIATIONS	1.5 TO 1

A signal characterization of CCD imagers includes the spectral responsivity, as illustrated in Figure 4.2.2-2, and the modulation transfer function (MTF). The MTF of a CCD imager consists of three components: aperture MTF, diffusion MTF, and the charge transfer MTF. The aperture MTF is the spatial frequency response associated with the geometry of the detector's collection aperture or photo-site. The one-dimensional representation is described by the familiar sinc function:

$$MTF_A(\nu) = \frac{\sin(\pi\nu d)}{\pi\nu d}$$

where  $\nu$  is spatial frequency (cycles/mm) and  $d$  is the size of the aperture.

The diffusion MTF accounts for the degradation in response due to the diffusion of photo-generated minority charge carriers from their point of origin in the substrate to their destination in the depletion region. Since this mechanism is a strong function of wavelength ( $\lambda$ ), the MTF is described as a function of both spatial frequency and wavelength:

$$MTF_D(\nu, \lambda) = \frac{1 - [\exp(-\alpha L_D)/(1+\alpha L)]}{1 - [\exp(-\alpha L_D)/(1+\alpha L_0)]}$$



where

$$\begin{aligned} \alpha &= \text{Spectral absorption coefficient of silicon,} \\ L_D &= \text{Depletion width,} \\ L_0 &= \text{Diffusion Length,} \\ L &= \left( \frac{L_0^2}{1 + L_0^2 \nu^2} \right) \end{aligned}$$

The charge transfer MTF accounts for the inefficiency in transferring charge during the readout process and can be written as:

$$MTF_{ct}(\nu) = e^{-N\epsilon(1 - \cos 2\pi p\nu)}$$

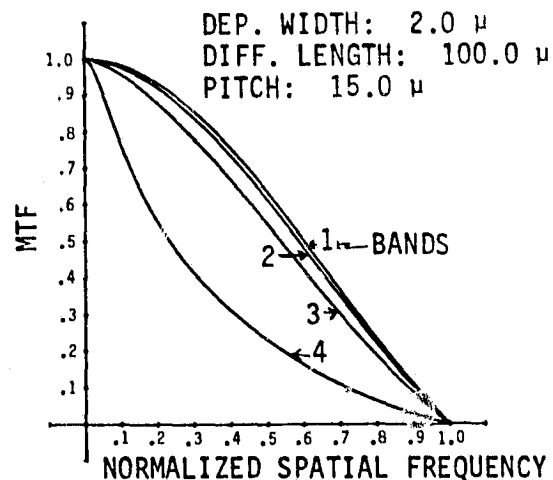
where

$$\begin{aligned} N &= \text{Number of transfers,} \\ \epsilon &= \text{Per transfer efficiency,} \\ p &= \text{Sensor pitch.} \end{aligned}$$

With the excellent charge transfer efficiency displayed by these devices (0.9999) and the small number of transfers per chip (less than 400 for a three phase device), the MTF loss due to charge transfer is negligible (i.e.,  $MTF_{ct} = 1$ ).

The spectrally weighted MTF for this sensor is plotted in Figure 4.2.2-3 against normalized spatial frequency. The limiting normalized frequency is 0.5 and corresponds to the Nyquist frequency of 33.3 c/mm.

These arrays utilize correlated double sampling to remove the Nyquist noise from the reset switch-output capacitance combination, and to suppress surface state and 1/f noise. This technique yields excellent dark noise performance of 20 - 30 rms electrons at 300°K.



SENSOR MTF vs SPATIAL FREQUENCY

Figure 4.2.2-3

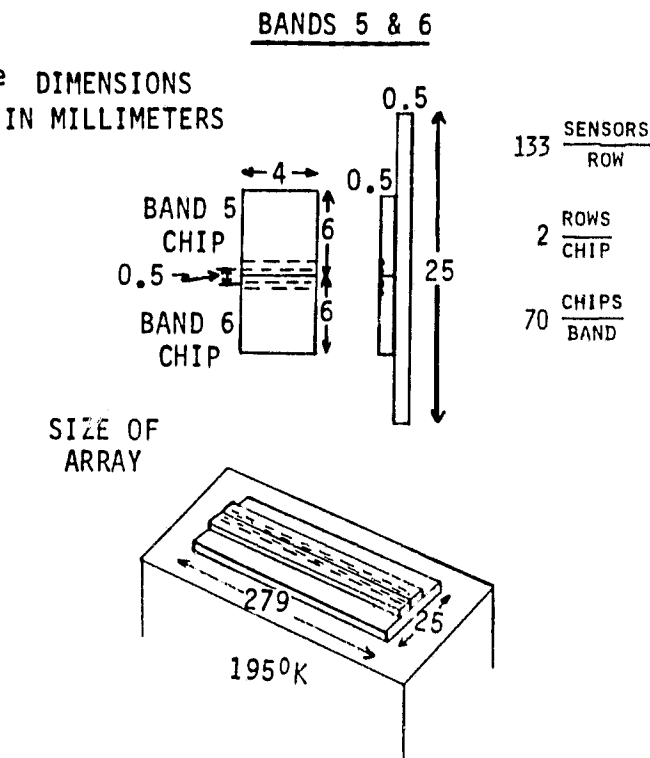


4.2.3 Detectors for the SWIR Bands: Bands 5 and 6

4.2.3.1 Configuration - The baseline detector array for the short wave infrared bands--1.55 to 1.75 microns and 2.1 to 2.4 microns, respectively--evolved from discussion with personnel at Honeywell Electro-Optical Center in Lexington, Massachusetts. The focal plane, shown in Figure 4.2.3-1, consists of two

linear arrays butted together to achieve inherent, band-to-band registration; the arrays have an in-track center-to-center spacing of 0.5 mm. Each array consists of 70 individual chips or subarrays. The chips contain two parallel rows of detectors that operate in the time delay and integrate (TDI) mode. The two rows are separated by 5.0 microns and contain 133 detectors each. The two element TDI configuration was suggested by Honeywell as a means for improving their manufacturing yield. In this configuration a chip will function even if one of the two TDI sensors is defective. The focal plane, therefore, consists of two linear TDI arrays, each containing 9,310 TDI detectors or, equivalently, 18,620

individual detectors. The detectors are photovoltaic, mercury-cadmium-telluride (HgCdTe) photodiodes with a long wavelength cutoff of 2.5 microns. The diodes are interfaced with a CCD shift register for readout. The detector aperture is 25 microns by 25 microns and the cross-track pitch is 30 microns. The relatively large in-track separation between the bands (0.5 mm) allows for a filter plate separate from the arrays. A transparent substrate containing both spectral filters would be located in close proximity to the arrays and aligned with their axis. As was the case with the visual array chips, laser beam trimming of these chips is necessary and will result in one dead TDI



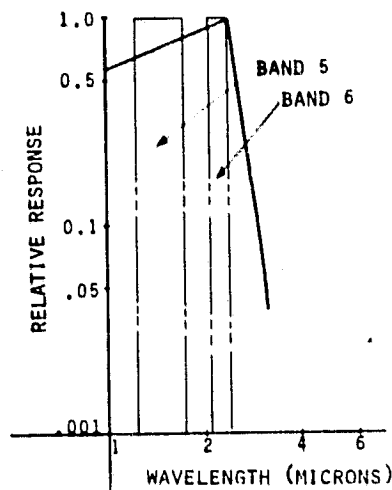
BASELINE FOCAL PLANE ARRAY  
FOR BANDS 5 AND 6

Figure 4.2.3-1



sensor at each end of a chip. A cold finger connected to a space radiator is located beneath the chips. Consequently, the signal processing electronics, with the exception of the CCD shift registers and low level multiplexers, are remotely located. The signal processing electronics are similar to that previously described for the visual arrays.

4.2.3.2 Detector Characteristics - The normalized spectral responsivity of the SWIR detectors is illustrated in Figure 4.2.3-2 along with the spectral bandpass for Bands 5 and 6. The detector characteristics for these arrays are listed in Table 4.2.3-1.



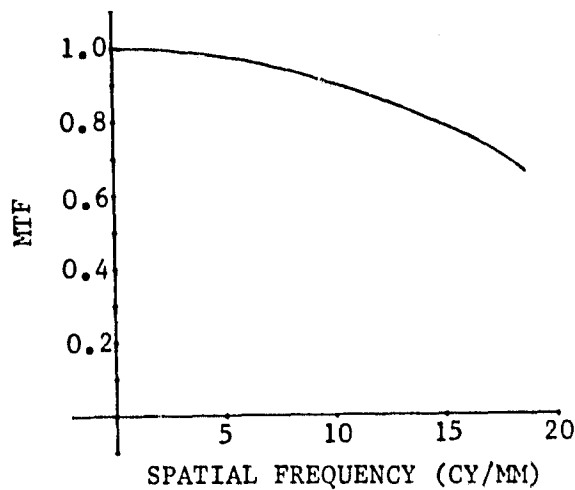
*HgCdTe SPECTRAL RESPONSIVITY*

*Figure 4.2.3-2*

<i>Table 4.2.3-1</i>	
<i>PV, HgCdTe DETECTOR CHARACTERISTICS</i>	
APERTURE	25 $\mu$ x 25 $\mu$
PITCH	30 $\mu$
D* (195 <sup>0</sup> K)	7.5x10 <sup>10</sup>
DARK CURRENT VARIATIONS	3 TO 1
GAIN VARIATIONS	1.5 TO 1

These detectors are characterized by their spectral responsivity, as illustrated in Figure 4.2.3-2, their MTF, and their detectivity, D\*. The MTF is simply the aperture response, sinc ( $\pi v d$ ), and is shown in Figure 4.2.3-3. The detectivity, D\*, which is a function of many parameters, can be written as

$$D^* = \frac{\lambda n q}{hc} \left[ \frac{4kT}{R_0 A} + 2q^2 n \phi_T \right]^{-1/2}, \text{ cmHz}^{1/2}/\text{w}$$



SWIR SENSOR MTF

Figure 4.2.3-3

where

$n$  = Quantum efficiency, typically 0.8

$q$  = Electronic charge

$h$  = Planck's constant

$c$  = Speed of light

$T$  = Temperature,  $^{\circ}\text{K}$

$k$  = Boltzmann's constant

$A$  = Detector area

$R_0$  = Dynamic impedance at zero bias

$\phi_T$  = Total photon flux, photons/  
 $\text{cm}^2\text{-sec}$

$\lambda$  = Wavelength

The total photon flux,  $\phi_T$ , consists of two components, the signal flux  $\phi_s$ , and the parasitic flux,  $\phi_p$ . The parasitic flux is the non-signal flux associated with the background radiation from the interior of the spacecraft and the heat conducted by the detector leads.  $\phi_T$  can be written as

$$\phi_T = \frac{T_0 \lambda H_s}{4hc f\#^2} + \frac{\lambda H_p}{hc}, \text{ photons/cm}^2\text{-sec}$$

where

$T_0$  = Transmittance of the optics

$f\#$  = Optical  $f$ -number

$H_s$  = Signal irradiance

$H_p$  = Parasitic irradiance

While not explicitly shown, detectivity is a strong function of temperature which is influenced principally by the temperature dependence of the intrinsic carrier concentration. This temperature dependence manifests itself through  $R_0$ ,

$$R_0(T) \sim e^{E_g/\beta kT}$$

where  $E_g$  is the bandgap energy, and  $\beta$  is a constant between 1 and 2 that depends on the generation-recombination process. This temperature dependence

plays an important role in selecting the operating point as well as in determining the degree of temperature control.

### 4.3 CONFIGURATION

The general configuration of the principal telescope is shown in Figure 4.3-1. The telescope consists of forward and aft modules which contain the Schwarzschild telescope assembly and the stereo mirror assembly, respectively. An assembly break between the modules permits vertical testing of the completed telescope assembly. As shown in the sketch, the telescope components are mounted to an internal invar or graphite-epoxy metering structure which is protected thermally by a thin aluminum shield. The three mirrors of the telescope and the stereo mirror are of frit-bonded, ULE, lightweight construction and are factory-aligned and focused. The thermal control tolerances and the thermal coefficients of the mirrors and the metering structure have been selected to assure that the rather liberal focus and alignment tolerances, discussed in Section 4.1.2, are maintained.

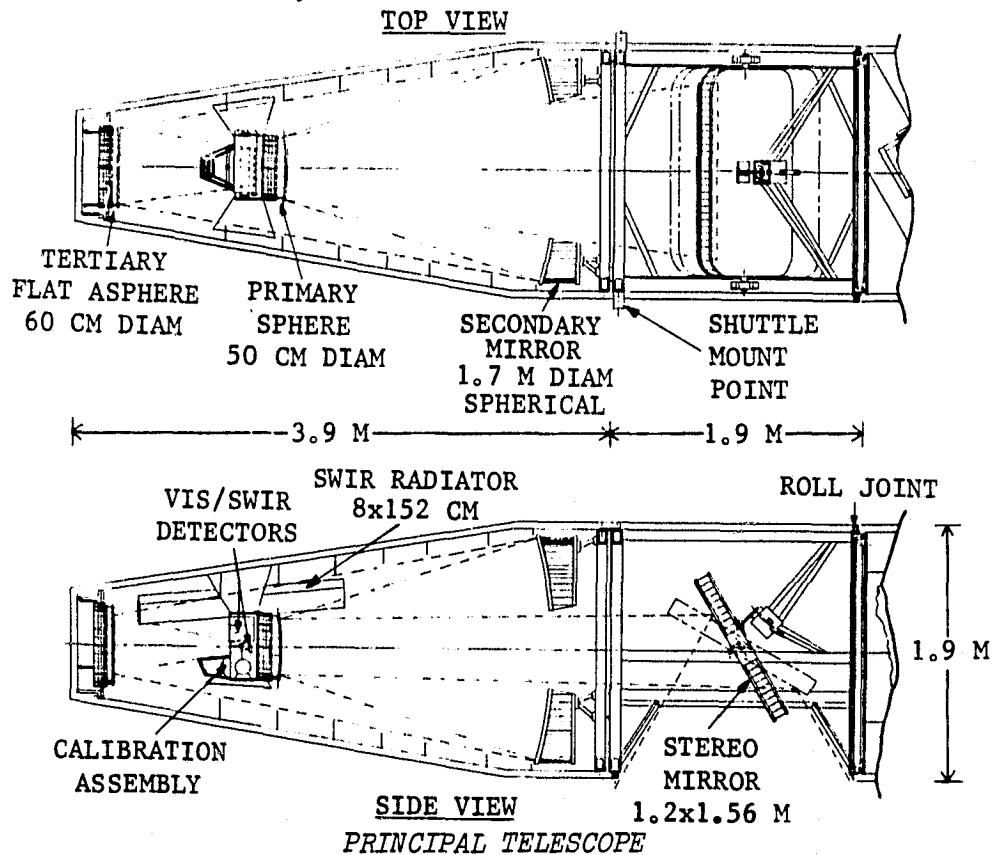
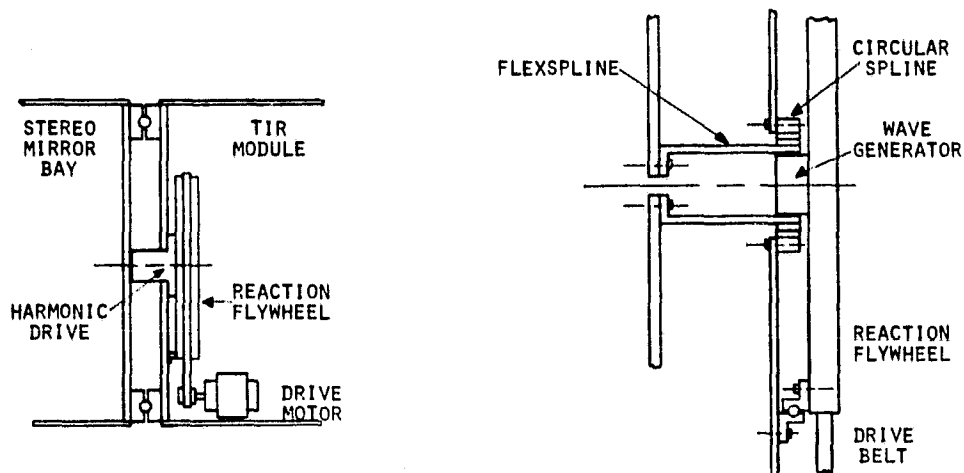


Figure 4.3-1

The stereo mirror assembly consists of the mirror, its mounts, and a drive which permits selection of the three stereo positions. The stereo mirror assembly is designed with internal compensation so that no dynamic disturbances are induced in the vehicle when the mirror position is changed.

A roll joint design concept is shown in Figure 4.3-2. The roll joint provides the capability for indexing the swath coverage, plus or minus three swath widths from its nominal position, for a total range of 1295 km (700 nm). The roll joint includes a reaction flywheel tuned to compensate the principal telescope's moment of inertia.



ROLL JOINT DESIGN CONCEPT

Figure 4.3-2

Because of the reliability considerations, no door closure is provided for the stereo mirror bay. Prior to shuttle ejection it is expected that this opening will be protected by a compliant seal incorporated into the shuttle retention cradles.

The major components of the principal telescope and first order estimates of their respective weights are listed in Table 4.3-1.

COMPONENT	MATERIAL	ESTIMATED WEIGHT (KG)
STEREO MIRROR	FRIT BONDED ULE	63
PRIMARY MIRROR	FRIT BONDED ULE	3
SECONDARY MIRROR	FRIT BONDED ULE	115
TERTIARY MIRROR	FRIT BONDED ULE	5
ROLL JOINT	ALUMINUM	159
SUPPORT STRUCTURE*	ALUMINUM AND GRAPHITE/EPOXY	475
MIRROR MOUNTS*	GRAPHITE/EPOXY	30
THERMAL SHIELD	ALUMINUM	100
OTHER		200
	TOTAL	1150 KG

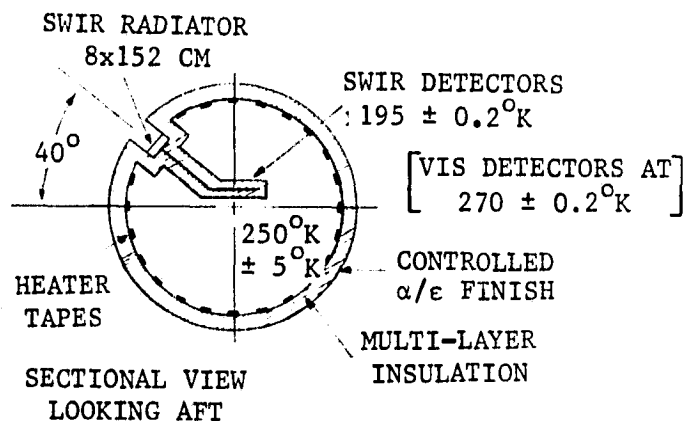
*\*If invar is used instead of graphite/epoxy, these weights become 852 and 56 kilograms, respectively.*

#### 4.4 THERMAL CONTROL

The thermal control system must provide an environment suitable for effective operation of the visible and short wavelength infrared linear arrays and their supporting electronics. Figure 4.4-1 shows the general thermal control approach for the principal telescope.

The temperature of the enclosure is passively cooled below  $250^{\circ}\text{K}$  by

selection of an appropriate exterior finish. The metering structure temperature is then regulated to  $250^{\circ}\text{K} \pm 5^{\circ}\text{K}$  by a system of heater tapes and controllers. The detector arrays are also regulated by sets of internal heaters. The SWIR detectors are attached by a high conductivity coupling to a space radiator



PRINCIPAL TELESCOPE THERMAL CONTROL

Figure 4.4-1

that is recessed into the West-facing wall and is shielded from exposure to direct or reflected sunlight and from the Earth albedo. Further analysis is required to determine whether an effective set of shields and baffles can be devised to allow operation of the short wavelength IR arrays over the full range of roll pointing. The space radiator shown in the sketch is sized for a heat rejection load of about 2.0 watts.

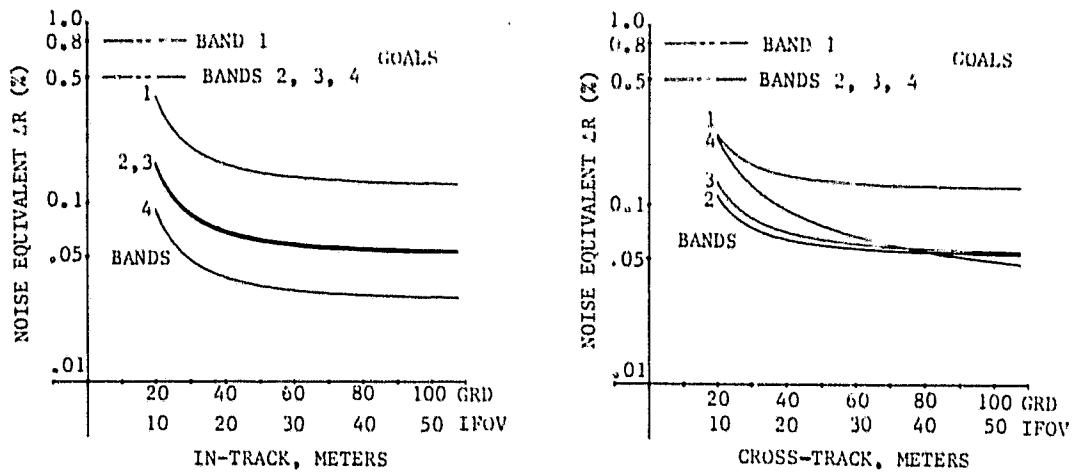
Note in Figure 4.3-1 that there is no door provided for closure of the stereo mirror bay between operating periods. Heat loss or gain through this opening for typical orbital cycles must be estimated before establishing the specific design of the thermal control system and estimating heater power requirements. This analysis, as well as analysis of the space radiator, should be conducted early in any follow-on study.

#### 4.5 PERFORMANCE ESTIMATES

Performance goals for the principal telescope were based on the radiometric performance goals of the thematic mapper. The assumed scene characteristics for each spectral band are discussed in Section 3.1. In-track and cross-track performance estimates for each band were calculated, using the optical performance characteristics given in Section 4.1 and the detector characteristics given in Section 4.2. Figure 4.5-1 shows the estimated noise equivalent incremental reflectance as a function of the ground resolved distance and IFOV for each visible band. These estimates are for the detected signal at the array and do not include the effects of quantizing or data processing at the ground station. For all cases, the design margin appears fully adequate.

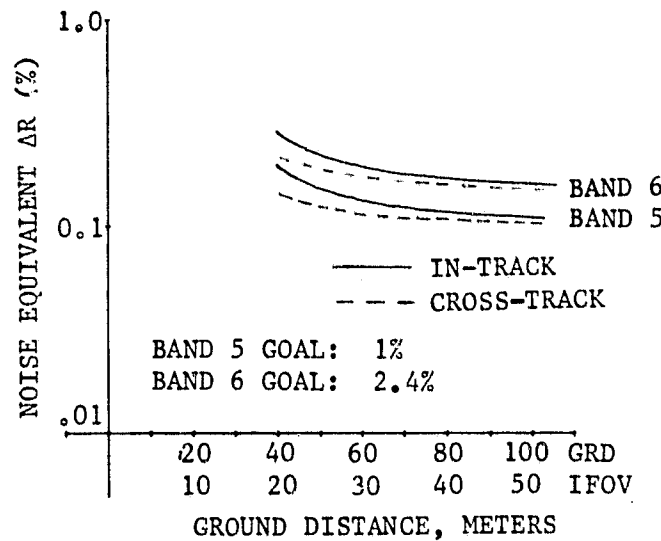
Similar estimates were made for the short wavelength infrared bands; the results are shown in Figure 4.5-2. In these cases, the assumed detector size of 30 micrometers limits the IFOV to 20 meters. The design margins appear to be fully adequate.





PERFORMANCE FOR VIS TELESCOPE

Figure 4.5-1



PERFORMANCE FOR SWIR TELESCOPE

Figure 4.5-2



#### 4.6 COVERAGE CHARACTERISTICS

In the normal operating mode of the principal telescope, monoscopic coverage of a 185 km (100 n.m.) swath can be selected anywhere within  $\pm 650$  km of the ground track (e.g., anywhere between New York and Chicago). The four visible arrays sample the image sequentially with a delay of about 2.0 milliseconds between bands. (This delay must be recognized if multispectral photographs are reconstructed at the ground station.) With the field sharing optics discussed previously, the short wavelength infrared bands sample the scene about two seconds after the visible bands. If this time lag proves undesirable, it could be eliminated by introducing a dichroic beam splitter with only a modest loss of light transmission.

Stereo coverage is accomplished by indexing the stereo mirror. Three positions are provided:  $15^{\circ}$  forward, vertical and  $15^{\circ}$  aft. Overlapping coverage, assuming 10 seconds are allowed for moving and settling the mirror, is about 325 km for the extreme stereo position, and about 130 km for either extreme and the zero positions.

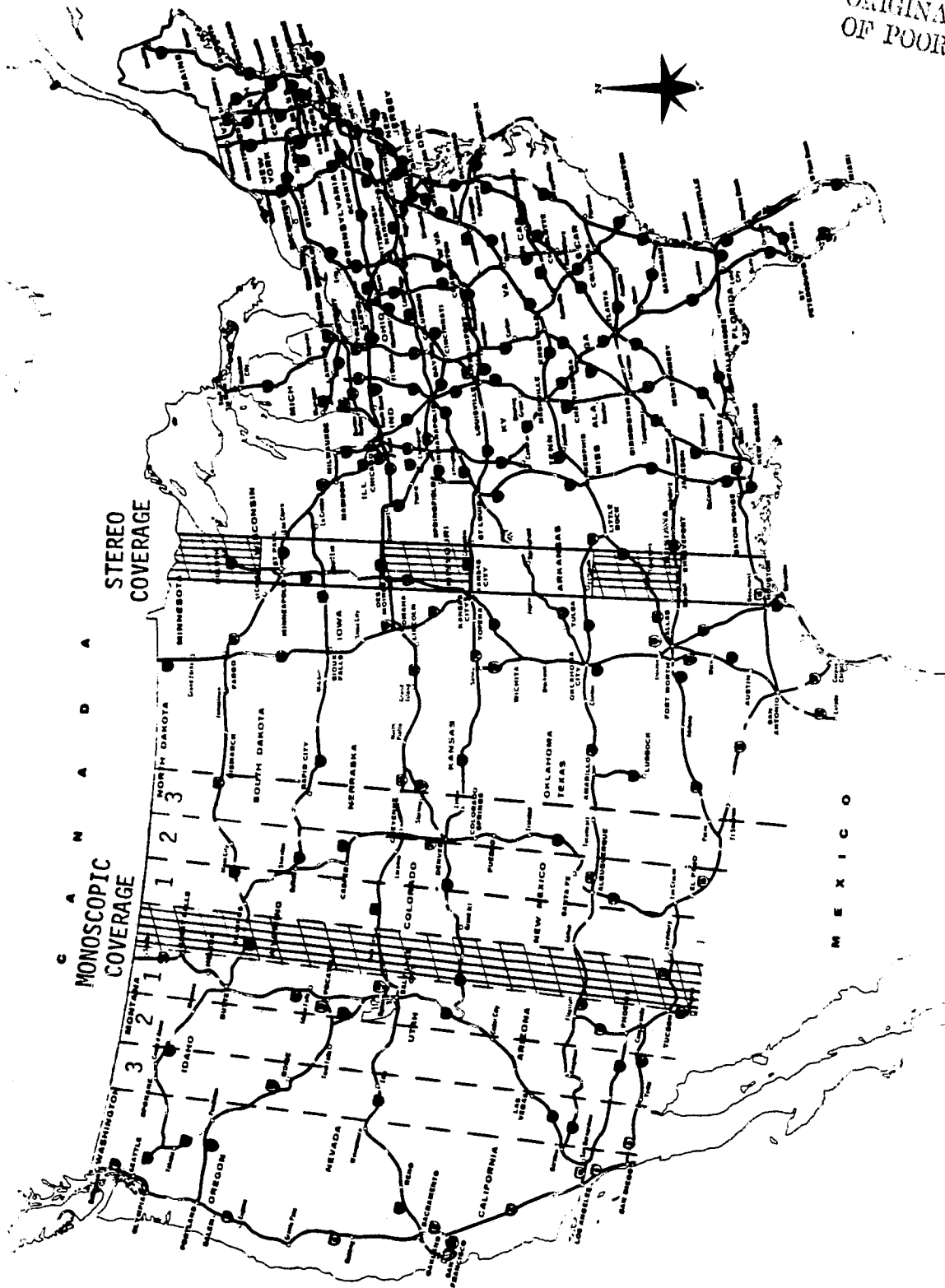
Lateral pairs are accomplished by rolling the principal telescope at the same time that the stereo mirror is indexed. Coverage characteristics are the same as for stereo pairs.

Lateral triplets are accomplished by rolling the principal telescope as the stereo mirror is indexed from  $-15^{\circ}$  to the zero position, then repeating the roll maneuver as the stereo mirror is indexed from zero to  $+15^{\circ}$ . The maximum length of contiguous coverage for this operation is about 130 km.

Figure 4.6-1 shows typical monoscopic and stereo coverage patterns for passes over the United States. In the monoscopic case shown, the zero roll position was selected. In the stereo case, the intervals between frames are required to index the stereo mirror from  $+15^{\circ}$  to  $-15^{\circ}$ .



ORIGINAL PAGE IS  
OF POOR QUALITY



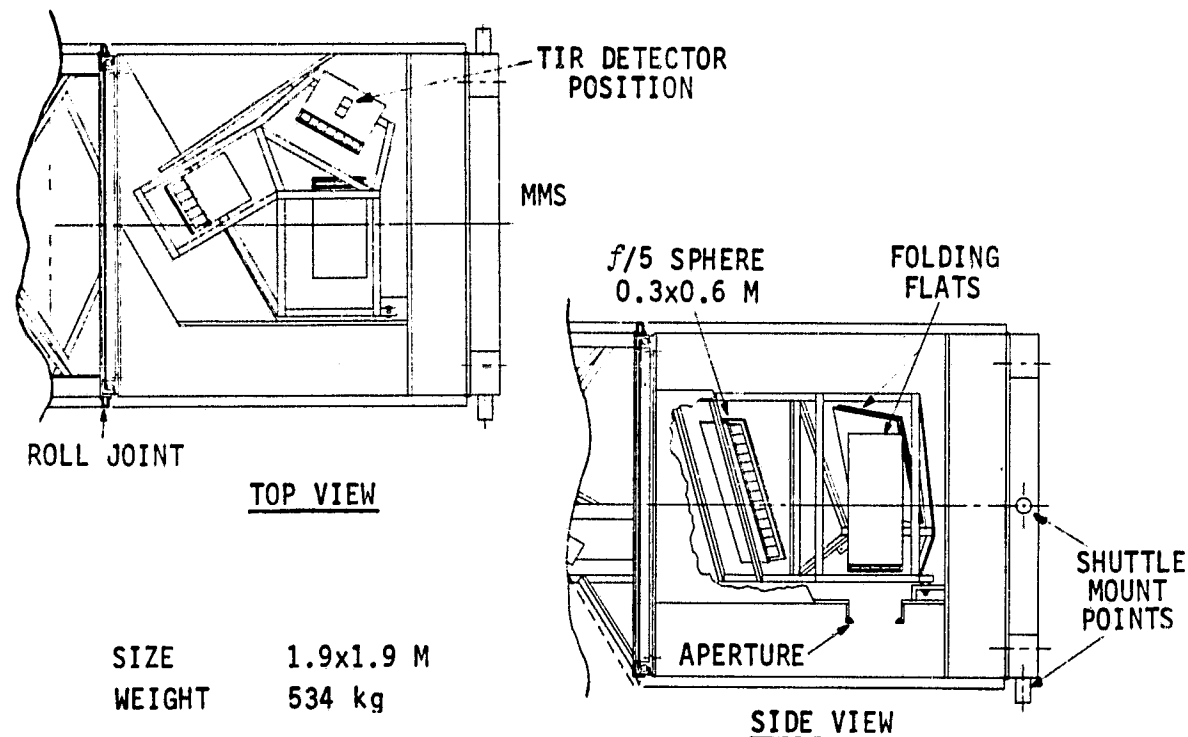
TYPICAL COVERAGE PATTERNS

Figure 4.6-1



## 5.0 DESIGN APPROACH FOR THERMAL INFRARED TELESCOPE

The selected design approach for the thermal infrared (TIR) telescope is described in this section. The TIR telescope is a module which is inserted between the principal telescope and the MMS, as shown in figure 5.0-1. The TIR telescope is comprised of the telescope optics and support structure; the associated electronic and thermal control components; and an outer shell, into which is mounted a large space radiator that cools the TIR detector array.



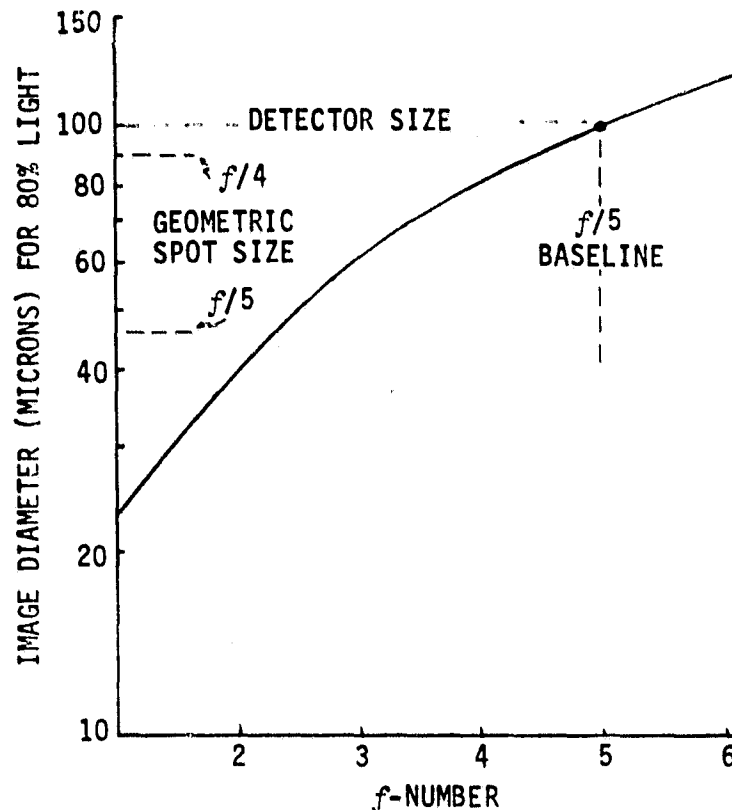
TIR TELESCOPE

Figure 5.0-1

### 5.1 OPTICS

The baseline "lens-less Schmidt" telescope is simply a spherical mirror with a field stop at its center of curvature. Two folding mirrors have been added to allow the detector array at the focal surface to be mounted directly to a space radiator. This type of optical system can provide essentially diffraction-limited performance over the required  $\pm 7.5^\circ$  field at thermal infrared wavelengths.

Figure 5.1-1 shows image spot diameters resulting from diffraction as a function of  $f$ -number. Superimposed on the chart are spot diameters resulting from geometric aberrations at  $f/4$  and  $f/5$ . These curves indicate that an  $f/5$  system is an appropriate choice for use with the 100 micrometer detectors selected for this spectral band.



DIFFRACTION IMAGE SIZE  
AT WAVELENGTH  $11.5 \mu$

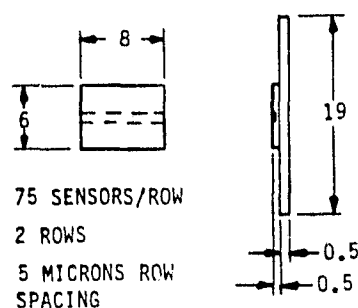
Figure 5.1-1

## 5.2 DETECTORS FOR THE TIR BAND: BAND 7

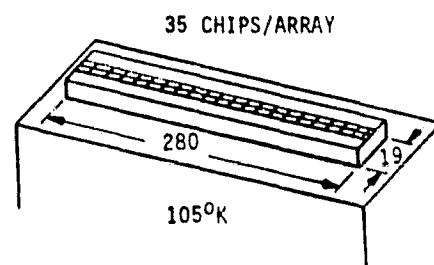
### 5.2.1 Configuration

Personnel at Honeywell Electro-Optical Center suggested the following detector array baseline for the 10.5 micron to 12.5 micron thermal infrared band. The focal plane, shown in Figure 5.2.1-1, consists of 35 individual chips butted together. Each chip consists of two parallel rows of detectors that operate in the TDI mode. The rows are separated by 5 microns and contain 75 photo-

voltaic mercury-cadmium-telluride detectors which interface with CCD shift registers for readout. The focal plane, therefore, consists of one linear TDI array containing 2625 TDI detectors or, equivalently, 5,250 individual detectors. The detector aperture is 100 microns by 100 microns and the cross-track pitch is 105 microns. A multilayer filter deposited on a transparent substrate is used to obtain the desired spectral bandpass. The need for laser trimming of the chips results in one dead TDI detector at each end of a chip. As in the SWIR focal plane, a cold finger, which is attached to a space radiator, is located directly beneath the chips and cools them to an operating temperature of 105°K. Similarly, the signal processing electronics, with the exception of the CCD shift registers and low level multiplexers, are remotely located. The processing is also similar to that used for the visual array.



DIMENSIONS IN  
MILLIMETERS



HONEYWELL DATA

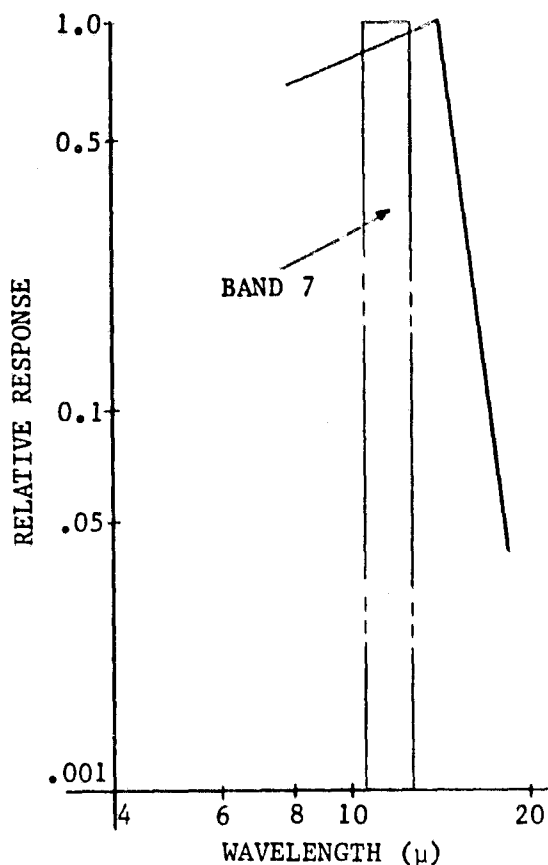
HgCdTe - PHOTOVOLTAIC  
CCD ARRAY - 5250 SENSORS  
100x100 MICRON SENSORS  
105 MICRON PITCH  
 $D^* = 1.5 \times 10^{10}$  @ 105°K

*TIR DETECTORS*

*Figure 5.2.1-1*

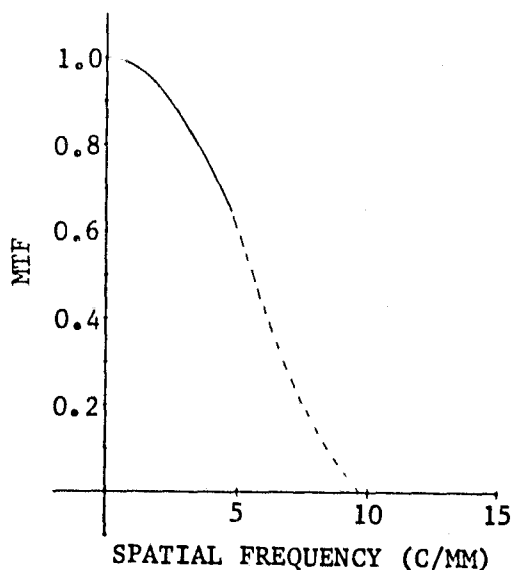
### 5.2.2 Detector Characteristics

The normalized spectral responsivity for these detectors, as well as the spectral bandpass for the thermal band, are illustrated in Figure 5.2.2-1. The detectors have a long wavelength cutoff of 14.8 microns. The detector characteristics are listed in Table 5.2.2-1.



NORMALIZED SPECTRAL RESPONSIVITY

Figure 5.2.2-1



TIR DETECTOR MTF

Figure 5.2.2-2

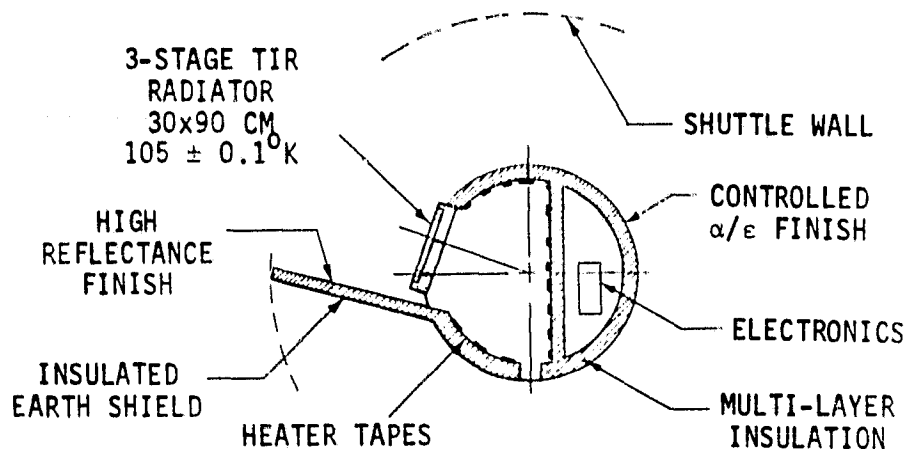
Table 5.2.2-1 TIR PV, HgCdTe DETECTOR CHARACTERISTICS	
APERTURE	100 $\mu$ x 100 $\mu$
PITCH	105
D* (105°K)	1.5x10
DARK CURRENT VARIATIONS	3 TO 1
GAIN VARIATIONS	1.5 TO 1

Spectral responsivity, MTF, and detectivity characterize these detectors similar to the SWIR detectors. The MTF consists of two components: sinc ( $\pi v d$ ) for the aperture MTF; and the diffusion MTF. Because Honeywell could not supply diffusion MTF information, only the aperture MTF (shown in Figure 5.2.2-2) was used to characterize the spatial response of these detectors. Similarly, Honeywell would not elaborate on D\*'s dependence on temperature or other parameters but referenced the NASA-Goddard Space Flight Center RFP No. -5 48729/254 instead.

### 5.3 THERMAL CONTROL

The thermal control system for the TIR telescope must provide a low temperature enclosure for the TIR optics and a very low temperature space radiator for the detector array. Figure 5.3-1 shows the

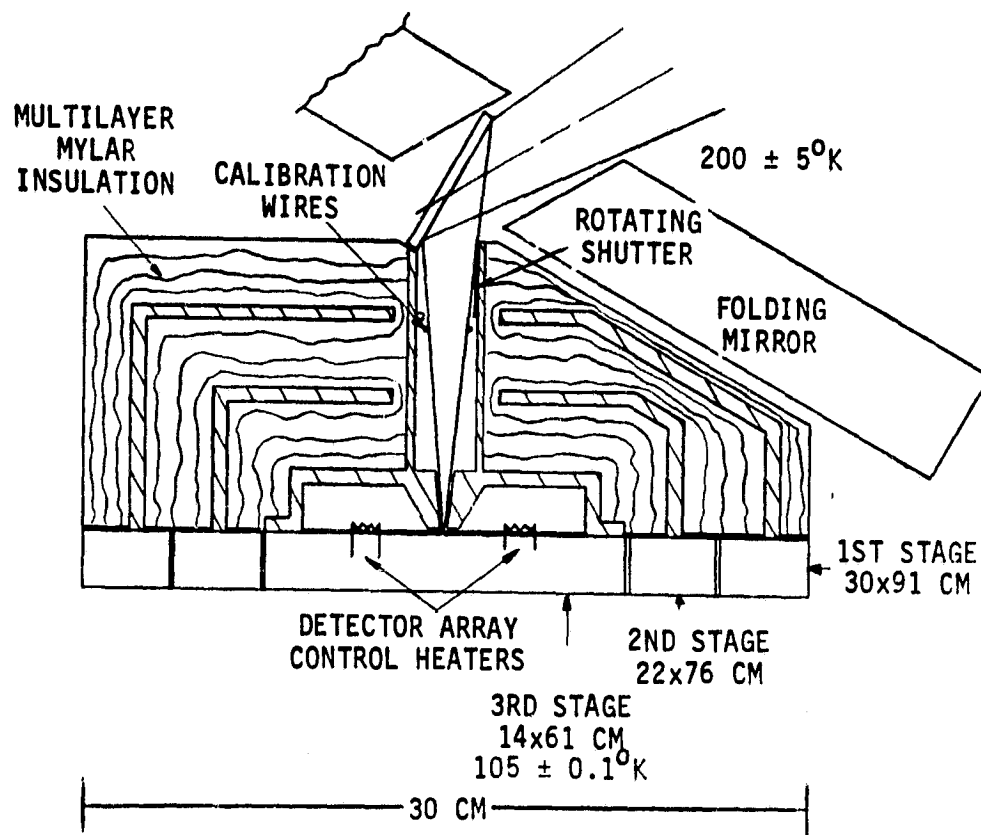
general thermal control approach for the TIR telescope. In this approach, the optical components are mounted within a heavily insulated enclosure which is designed for an equilibrium temperature of about  $200^{\circ}\text{K}$ . A space radiator is mounted on the dark (West) side of the enclosure. An Earth shield protects the space radiator from albedo radiation from the Earth's surface. The space radiator is sized for a heat rejection load of approximately 0.45 watts.



*TIR THERMAL CONTROL*

*Figure 5.3-1*

Figure 5.3-2 shows a design concept for the TIR detector and space radiator assembly. In this concept the detector array is mounted, via a cold finger, to the innermost and coldest of a three-stage space radiator. The view factor of the detectors is constrained by a thermal baffle into which are mounted a pair of calibration wires and a capping shutter. The dimensions shown are based on estimates of the combined heat rejection requirements for heat transmitted into the detector assembly from the  $200^{\circ}\text{K}$  enclosure, heat from the ground scene, and heat from power dissipation within the detectors and their associated electronics. Control heaters are provided in the detector assembly to maintain the operating temperatures within  $\pm 0.1^{\circ}\text{K}$  of the nominal  $105^{\circ}\text{K}$  detector temperature.



THERMAL CONTROL FOR TIR DETECTORS

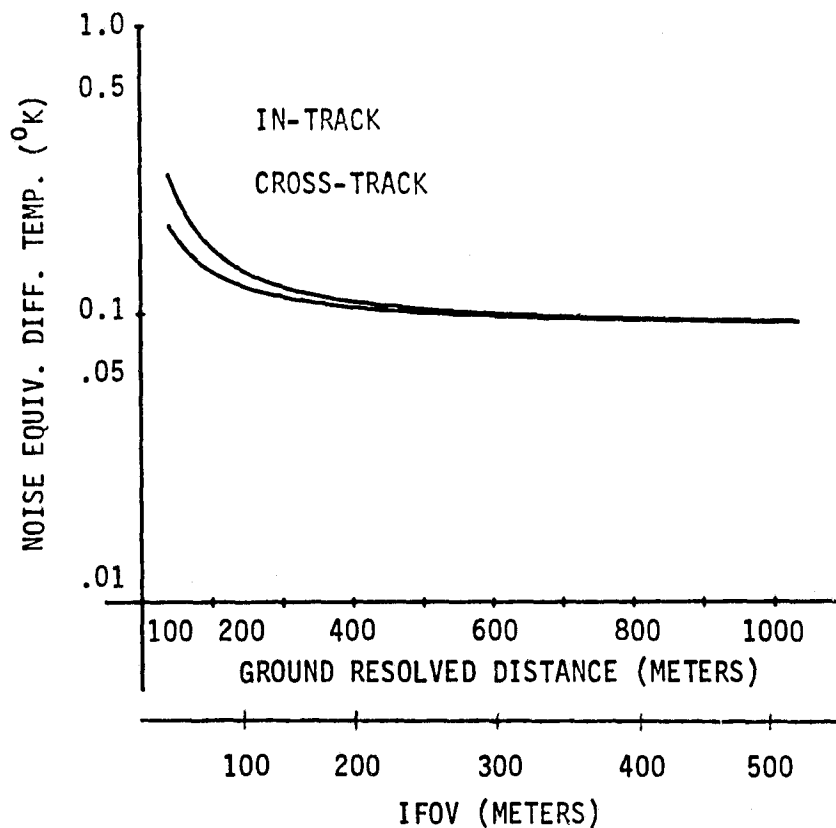
Figure 5.3-2

Temperature sensitivity of the TIR optics is not a significant factor in the design. The depth of focus of the optical system is in excess of 1000 micrometers while the change in focus of a one-meter focal length, ULE mirror between factory ambient and  $200^{\circ}\text{K}$  is less than 10 micrometers.

The aperture stop of the TIR telescope is located near the bottom of the thermal enclosure. A window of a suitable infrared material (ZnS or ZnSe) and a blocking filter can be provided to prevent albedo heat from entering the optical enclosure if heat balance studies show this to be desirable. If not, the TIR bandpass filter would be applied to the reflecting surface closest to the detector array.

## 5.4 PERFORMANCE OF THE THERMAL INFRARED TELESCOPE

The thermal infrared telescope provides monoscopic coverage of a 185 km (100 nm) cross-track ground swath directly below the spacecraft. Preliminary performance estimates indicate that the baseline  $f/5$  optics and 100 micrometer HgCdTe detectors should be capable of resolving temperature differences of less than  $0.5^{\circ}\text{K}$  between adjacent 70-meter samples, i.e.; the TIR band resolution should be essentially equivalent to the *visible* band resolution of the present MSS. (It should be noted that the TIR detectors cannot distinguish temperature differences from emittance differences. It has been assumed in the study that in the TIR band, the performance requirement applies to surface areas of similar emittance or repeat coverage of the same area.) Figure 5.4-1 plots the estimated in-track and cross-track noise equivalent temperature differences as a function of ground resolved distance and IFOV. These estimates are for the detectors alone and do not include noise contribution from quantizing and ground reconstruction.



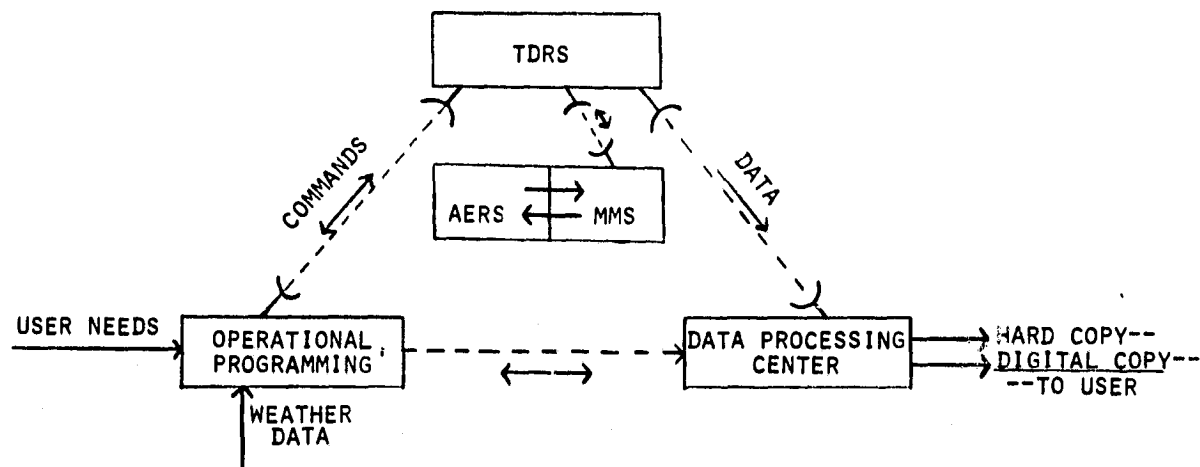
PERFORMANCE FOR TIR TELESCOPE

Figure 5.4-1



## 6.0 INTERFACE REQUIREMENTS

The Advanced Earth Resources Satellite (AERS) described in the previous sections is intended to be a payload for NASA's Multimission Modular Spacecraft (MMS). The spacecraft will be launched by the shuttle into low-Earth, polar orbit, and boosted into the final 705km circular orbit by the MMS. Operational commands will be relayed to the satellite by the Tracking and Data Relay Satellite (TDRS). Scene data will be transmitted from the MMS via the TDRS to the ground data processing center. These operational interfaces are shown in Figure 6.0-1. It should be noted that the operational programming for the AERS, because of its roll and stereo pointing capability, is more flexible than that of previous Landsat payloads. A ground command center will be needed to program the system in response to user needs, weather predictions and prior coverage feedback. A data processing center will receive and record the scene data from the AERS/MMS. The following sections discuss the data handling interfaces and the vehicle interfaces.

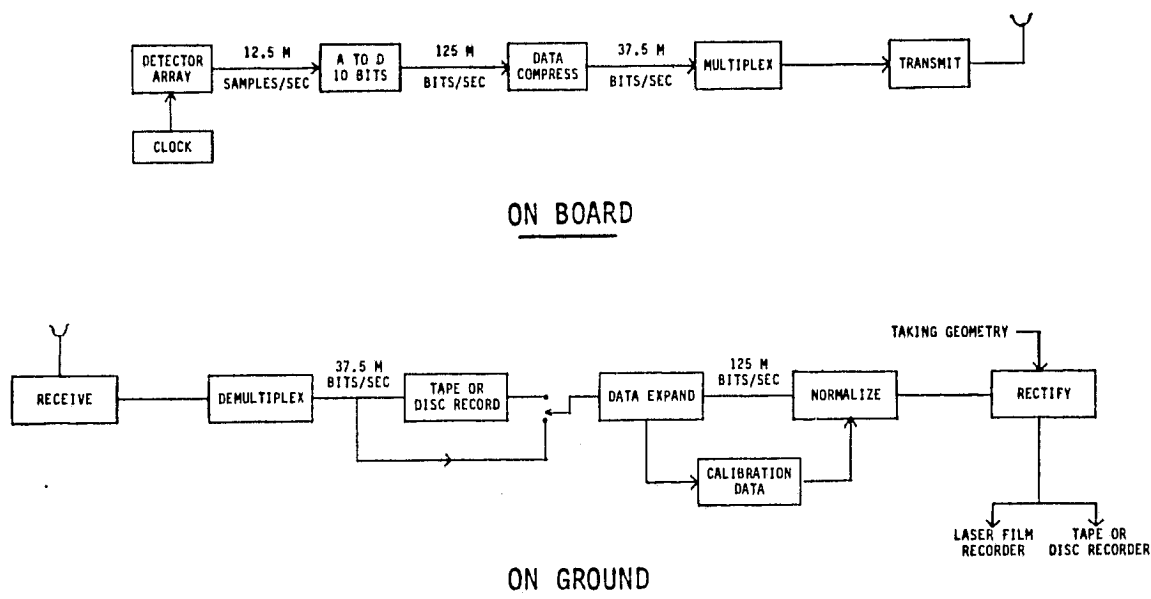


OPERATIONAL INTERFACES

Figure 6.0-1

## 6.1 DATA HANDLING INTERFACES

The signal from each of the detectors in the seven spectral bands is transmitted in real time to a ground data processing center. No full bandwidth on-orbit recording is provided, although this capability could be added if and when appropriate recorders are available or if reduced bandwidth (reduced resolution) delayed imagery is desired. Figure 6.1-1 shows a typical data flow from one of the visible arrays. In this flow the detector array is first sampled at the proper line rate to give a 10-meter GSD; the samples are then quantized at about 10 bits per pixel which is estimated to be adequate for the entire range of illumination conditions, target reflectances, and detector sensitivity variations.

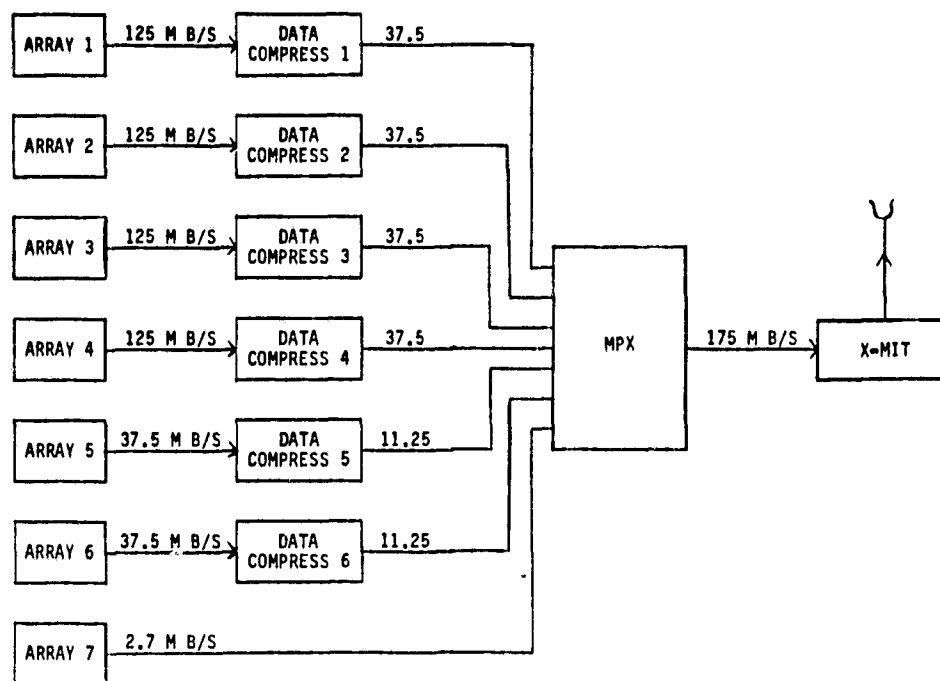


TYPICAL DATA FLOW  
(Each Visible Channel)

Figure 6.1-1

The bit stream is then compressed to approximately 3 bits per sample by delta modulation encoding, wherein each pixel is compared to the adjoining pixels and only the differences are transmitted. After compression, the seven channels of data are multiplexed and transmitted via the TDRS to the ground station. The multiplexer output is approximately 175 megabits/second which is well within

the capacity of one of the TDRS transponders. Figure 6.1-2 shows the combined on-board data flow for the full system.

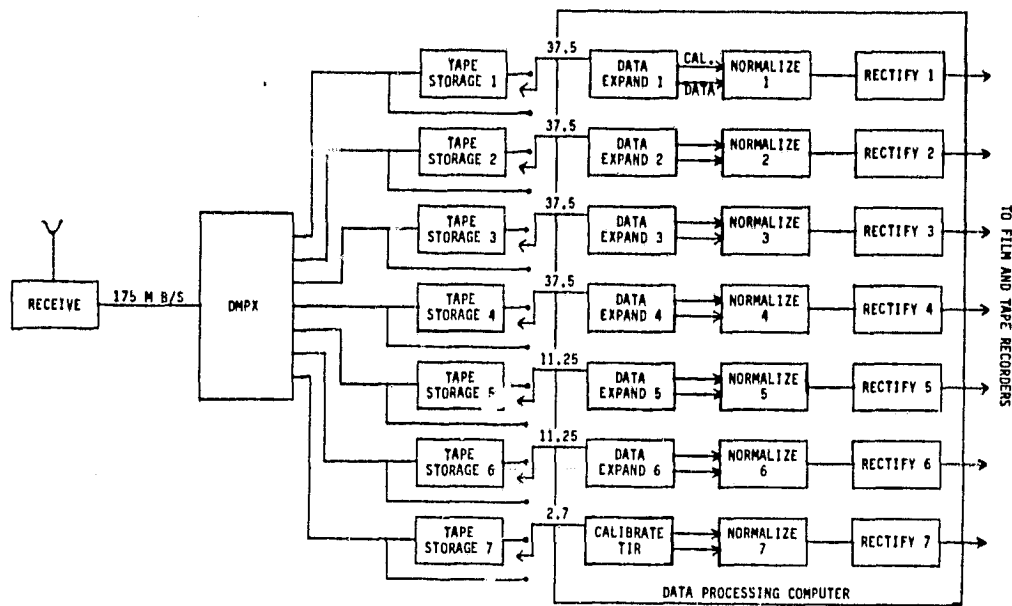


ON-BOARD DATA FLOW

Figure 6.1-2

On the ground the signal is demultiplexed into the seven channels of data, and recorded. The signal from the demultiplexer, or from the recorder, is expanded back to the original 10 bits per pixel and normalized by the previously stored calibration data recorded at the beginning of each operational pass. The corrected data is then rectified to remove the known effects of lens distortion and any geometric distortion resulting from the pointing geometry. Finally, the corrected data is recorded either in digital form or as a visual image on high resolution film. The combined on-ground data flow for the complete system is shown in Figure 6.1-3.

The digital data rates for the AERS are about seven times those of the thematic mapper. These rates pose a formidable data processing and recording problem. There is an obvious need to establish specific requirements for operational data handling from which realistic assessments can be made of the cost, schedule and technology development requirements for the data processing hardware and support software.

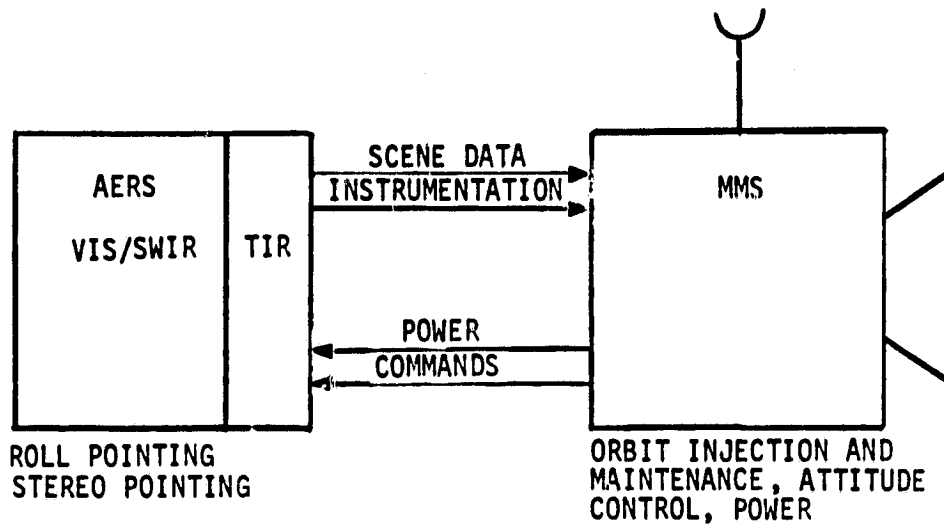


ON-GROUND DATA FLOW

Figure 6.1-3

## 6.2 VEHICLE INTERFACES

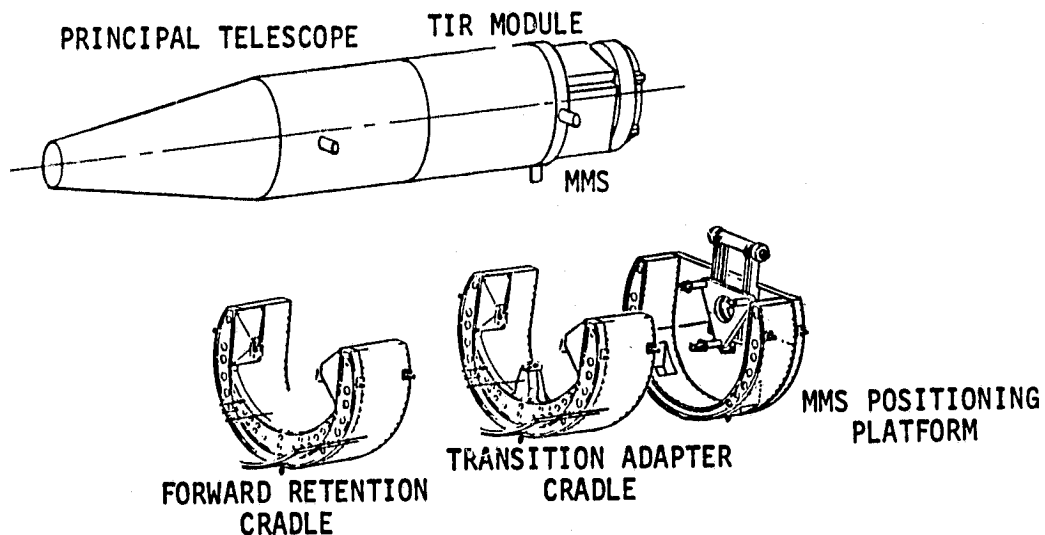
The functional interfaces between the MMS and AERS are shown in simplified form in Figure 6.2-1. In general, it is expected that the MMS will provide orbit injection, maintenance and deboost; attitude control (fixed Earth orientation); power, telemetry and commands; and wideband data transmission, via the TDRS. All of the requirements for orbit adjust and attitude control appear to be well within the capabilities of the MMS with a PM-II propulsion subsystem. Power requirements, exclusive of the data link, should be under 500 watts during daylight operation or, perhaps, 100 watts if the thermal telescope is operated on the dark side of the orbit. These values are also well below the MMS capacities. The only interface requirement not met by current MMS subsystems is the wideband (175M b/s) data link to the TDRS.



VEHICLE INTERFACES

Figure 6.2-1

The mechanical interface between the AERS and MMS has not been addressed in this study. There are no critical alignments or tolerances at the interface. The AERS stereo and roll drives are self-compensated so that attitude disturbances are not transmitted into the MMS. The mechanical interface, therefore, will be designed primarily from consideration of loads imposed during launch and shuttle ejection and retrieval. Figure 6.2-2 shows one preliminary concept for supporting the payload in the shuttle bay.



SHUTTLE MOUNTING PLAN

Figure 6.2-2



## 7.0 PROGRAM RISK ANALYSIS

### 7.1 PRINCIPAL TELESCOPE

The design concepts selected for the principal telescope are based in large part on known technology. All of the following technologies have been demonstrated successfully in prior NASA or DOD programs:

- Graphite epoxy structures
- Lightweight ULE or fused silica mirrors
- Mirror position drives
- Roll joints
- Passive space radiators
- On-board data processing

The technology for linear arrays of silicon CCD detectors, with characteristics required for Bands 1 - 4, is well advanced at Westinghouse\* and other sources. The specific array configuration selected as the baseline for this study, which incorporates the four rows of detectors with their respective filters onto each chip, has not yet been developed. An early feasibility demonstration of both the cell geometry and the filter deposition appears desirable.

The technology for the photovoltaic HgCdTe linear arrays for Bands 5 and 6 is under development at Honeywell and other sources. The technology for these detectors is similar to and less demanding than that required for the 1000-element, thermal infrared array development currently being sponsored by NASA/GSFC. Early demonstration of this detector technology is also desirable.

The calibration system for Bands 1 - 6 is a simple, multi-level, internal illuminator. The system provides relative calibration among the detectors, but does not provide an absolute through-the-optics calibration. Techniques for using known "ground truth" targets for establishing absolute reflectance calibration need to be established.

---

\*"Array Technology as Applied to Future Earth Resources Sensors", Hall and McCann, Westinghouse, May 1979, SPIE Vol. 183 Space Optics (1979).



No high risk technology developments have been identified for the principal telescope.

## 7.2 THERMAL INFRARED TELESCOPE

The optics, filter, and structure for the thermal infrared telescope are simple and undemanding. Data rates and data processing requirements for the thermal infrared band are considerably lower than for Bands 1 - 6.

The detector array selected for the thermal infrared band is based on the NASA/GSFC TIRA development. The detectors are 100-micrometer, square HgCdTe cells, operating in the photovoltaic mode to avoid chopping. Sensitivity, stability, and life characteristics of these detectors need to be established.

Thermal control of the TIR optics enclosure and of the space radiator require a combination of selective surfaces, thermal shields, and control heaters which should be based on a more thorough study of mission parameters than could be conducted during this brief study. A thermal model of the TIR telescope should be developed early in the program to determine the effects of mission variables on the thermal control system.

Calibration of the thermal detectors is performed by closing a capping shutter and energizing a pair of hot wires near the focal surface. This approach provides relative calibration of the detectors but does not provide absolute radiometric calibration of the system. Techniques for establishing absolute calibration, either by factory system tests or by use of "ground truth" targets on-orbit, need to be established.

## 7.3 GROUND STATION

The advanced earth resources satellite described in this study will collect and transmit to a ground station approximately 100 times as much data per second (or per unit ground area) as the previous Multi-Spectral Scanners. These data must be recorded for temporary storage, processed to eliminate known photometric and geometric distortions, and re-recorded on film, discs, or tape for distribution. A quick look at the data handling requirements



indicates that the requirements for data recording on film or tape can be met with existing laser and tape recorders. None of the data processing operations envisioned are, by themselves, particularly demanding. The combination of seven channels of data, all being processed at high rates in real time, does require a computer facility of major proportions. Development of the computer facility and the associated software should be conducted in parallel with the satellite development. Cost and schedule requirements for the ground station are expected to be very significant.

The amount of data to be recorded at the ground station will depend on the operational programming of the satellite system. Raw data from the satellite will be received at a rate of more than  $10^{10}$  bits per minute. If these data are stored on magnetic tape, appreciable storage volume will be required. An alternative storage media--optical disc recording--is under development at Kodak and several other sources. Disc data storage offers quicker data access than tape and requires less than one-tenth the storage volume. Continued development of optical disc technology should be encouraged for Landsat data recording.

